Article:
Meinhardt, A-K, März, C, Schuth, S et al. (4 more authors) (2016) Diagenetic regimes in Arctic Ocean sediments: Implications for sediment geochemistry and core correlation. Geochimica et Cosmochimica Acta, 188. pp. 125-146. ISSN 0016-7037

https://doi.org/10.1016/j.gca.2016.05.032

Elsevier Editorial System(tm) for Geochimica et Cosmochimica Acta

Manuscript Draft

Manuscript Number: GCA-D-15-00523R2

Title: Diagenetic regimes in Arctic Ocean sediments: Implications for sediment geochemistry and core correlation

Article Type: Article

Corresponding Author: Dr. Ann-Katrin Meinhardt,

Corresponding Author's Institution: Carl von Ossietzky University Oldenburg, Institute for Chemistry and Biology of the Marine Environment

First Author: Ann-Katrin Meinhardt

Order of Authors: Ann-Katrin Meinhardt; Christian März; Stephan Schuth; Karsten Lettmann; Bernhard Schnetger; Jörg-Olaf Wolff; Hans-Jürgen Brumsack

Abstract: Dark brown sediment layers are a potential stratigraphic tool in Quaternary Arctic Ocean sediments. They are rich in Mn, Fe, and trace metals scavenged from the water column and were most likely deposited during interglacial intervals. In this study, we combine sediment and pore water data from sediment cores taken in different parts of the Arctic Ocean to investigate the influence of early diagenetic processes on sediment geochemistry. In most studied cores, Mn, Co, and Mo are released into the pore waters from Mn oxide dissolution in deeper (>1.5 m) sediment layers. The relationship between sedimentary Mn, Co, and Mo contents in excess of the lithogenic background (elementxs) shows that Coxs/Moxs values are a diagnostic tool to distinguish between layers with diagenetic metal addition from the pore waters (Coxs/Moxs<1), layers affected by Mn oxide dissolution and metal release (Coxs/Moxs>10), and unaffected layers (Coxs/Moxs from 1 to 10). Steady-state calculations based on current pore water profiles reveal that in the studied cores, the diagenetic addition of these metals from the pore water pool alone is not sufficient to produce the sedimentary metal enrichments. However, it seems evident that dissolution of Mn oxides in the Mn reduction zone can permanently alter the primary geochemical signature of the dark brown layers. Therefore, pore water data and Coxs/Moxs values should be considered before core correlation when this correlation is solely based on Mn contents and dark sediment color. In contrast to the mostly non-lithogenic origin of Mn in the dark brown layers, sedimentary Fe consists of a large lithogenic (80%) and a small non-lithogenic fraction (20%). Our pore water data show that diagenetic Fe remobilization is not currently occurring in the sediment. The dominant Fe sources are coastal erosion and river input. Budget calculations show that Fe seems to be trapped in the modern Arctic Ocean and accumulates in shelf and basin sediments.
The Fe isotopic signal δ56Fe of the solid phase is positive (~0.2 to 0.3‰) in samples defined as the lithogenic background without significant Fe enrichments. With increasing non-lithogenic Fe contents in the sediment, δ56Fe becomes more negative, which indicates a shelf-to-basin export of an isotopically lighter Fe fraction. We assume that the same transport process is true for Mn.

Diagenetic regimes in Arctic Ocean sediments: Implications for sediment geochemistry and core correlation

A.-K. Meinhardt[a]*, C. März[b], S. Schuth[c], K. A. Lettmann[a], B. Schnetger[a], J.-O. Wolff[a], H.-J. Brumsack[a]

[a] Institut für Chemie und Biologie des Meeres (ICBM), Carl von Ossietzky Universität Oldenburg, 26111 Oldenburg, Germany (* corresponding author: ann.katrin.meinhardt@uni-oldenburg.de, +49-441-798-2534)

[b] School of Civil Engineering and Geosciences, Newcastle University, Newcastle upon Tyne NE1 7RU, United Kingdom

[c] Institut für Mineralogie, Leibniz Universität Hannover, 30167 Hannover, Germany

Abstract

Dark brown sediment layers are a potential stratigraphic tool in Quaternary Arctic Ocean sediments. They are rich in Mn, Fe, and trace metals scavenged from the water column and were most likely deposited during interglacial intervals. In this study, we combine sediment and pore water data from sediment cores taken in different parts of the Arctic Ocean to investigate the influence of early diagenetic processes on sediment geochemistry. In most studied cores, Mn, Co, and Mo are released into the pore waters from Mn oxide dissolution in deeper (>1.5 m) sediment layers. The relationship between sedimentary Mn, Co, and Mo contents in excess of the lithogenic background ($element_{xs}$) shows that Co_{xs}/Mo_{xs} values are a diagnostic tool to distinguish between layers with diagenetic metal addition from the pore waters ($Co_{xs}/Mo_{xs}<1$), layers affected by Mn oxide dissolution and metal release

(Co_{xs}/Mo_{xs}>10), and unaffected layers (Co_{xs}/Mo_{xs} from 1 to 10). Steady-state calculations based on current pore water profiles reveal that in the studied cores, the diagenetic addition of these metals from the pore water pool alone is not sufficient to produce the sedimentary metal enrichments. However, it seems evident that dissolution of Mn oxides in the Mn reduction zone can permanently alter the primary geochemical signature of the dark brown layers. Therefore, pore water data and Co_{xs}/Mo_{xs} values should be considered before core correlation when this correlation is solely based on Mn contents and dark sediment color. In contrast to the mostly non-lithogenic origin of Mn in the dark brown layers, sedimentary Fe consists of a large lithogenic (80%) and a small non-lithogenic fraction (20%). Our pore water data show that diagenetic Fe remobilization is not currently occurring in the sediment. The dominant Fe sources are coastal erosion and river input. Budget calculations show that Fe seems to be trapped in the modern Arctic Ocean and accumulates in shelf and basin sediments.

The Fe isotopic signal δ^{56}Fe of the solid phase is positive (~0.2 to 0.3‰) in samples defined as the lithogenic background without significant Fe enrichments. With increasing non-lithogenic Fe contents in the sediment, δ^{56}Fe becomes more negative, which indicates a shelf-to-basin export of an isotopically lighter Fe fraction. We assume that the same transport process is true for Mn.

Keywords

Arctic Ocean, sediment, pore water, diagenesis, manganese, iron isotopes, budget

1. Introduction

The Arctic Ocean plays an important role for the global climate because it impacts deep water formation in the North Atlantic and therefore the global overturning circulation (Aagaard et al., 1985). As the Arctic Ocean is very sensitive to climate change, research into the impacts of current global warming, sea ice melting and sea level rise has been intensified over the last decades (e.g., Lambeck et al., 2002; Anisimov et al., 2007). Sedimentary records are valuable archives of different climate conditions in the past, and the response of the Arctic Ocean to these conditions. Extraction of this information can provide unique insights into the past, and possibly future effects of changing environmental conditions in this highly sensitive environment. An important requirement for such studies is the establishment of an accurate age model for the sediments, which is an omnipresent problem in the Arctic environment (Alexanderson et al., 2014). The use of several conventional dating techniques in the Arctic (e.g., ^{14}C dating, $\delta^{18}O$ stratigraphy) is hindered by low organic matter contents in the basin sediments, poor preservation of calcareous tests, and problematic correlations of Arctic to lower latitude oxygen isotope records due to the changing fresh water contribution from Arctic rivers (Backman et al., 2004; Spielhagen et al., 2004). An alternative potential stratigraphic tool for core correlation in Quaternary Arctic sediments are widespread, cyclically occurring dark brown Mn-rich sediment layers. They seem to have formed during interglacial intervals by enhanced Mn input (Jakobsson et al., 2000; März et al., 2011; Meinhardt et al., 2014; recent review by Löwemark et al., 2014). In oxic waters Mn particles in the form of (oxyhydr)oxides are often associated with Fe (oxyhydr)oxides. During settling to the sea floor, these Mn- and Fe-rich particulates scavenge trace metals from the water column, creating parallel sedimentary enrichments in, e.g., Co, Mo, and Ni (Goldberg, 1954; März et al., 2011; 2012; Meinhardt et al., 2014). The dark brown layers may be used for core correlation if they were deposited synchronously across the whole

Arctic Ocean during interglacials (Löwemark et al., 2012, 2014). However, this stratigraphic use of the brown layers is only justified when significant diagenetic modification can be excluded. Dissolution and re-precipitation of Mn or Fe (oxyhydr)oxides and other sediment components after deposition have the potential to completely erase primary Mn layers, and form new Mn layers at the redox boundary in the sediment (e.g., Li et al., 1969; Burdige, 1993; Macdonald and Gobeil, 2012). These processes may disrupt the climatically forced sequence of Mn enrichments, and therefore prevent their use for stratigraphic purposes (Sundby et al., 2015).

In addition to these marked Mn enrichments, another prominent feature of Arctic Ocean sediments is the enrichment of Fe relative to average shale in different sediment layers. In sediment cores from the Mendeleev Ridge, many dark brown Mn-rich layers have elevated Fe contents as well, although the variations in Fe contents are less pronounced (März et al., 2011, 2012; Meinhardt et al., 2014). Particularly in Mendeleev Ridge surface sediments, Fe contents in excess of the lithogenic background (Fe_{xs}) are on the same order of magnitude (by weight) as Mn_{xs} contents (Meinhardt et al., 2014). However, despite significant progress in our understanding of Arctic Mn-, Fe-, and trace metal-rich layers, a more systematic investigation of these particular geochemical features is still missing. In this study, we combine solid phase and pore water data of sediment cores from different parts of the Arctic Ocean to determine which elements are currently influenced by dissolution/reprecipitation processes, and to what extent the location and composition of dark brown layers is modified by diagenesis. By analyzing Fe isotope ratios in selected sediment layers we will further extend our discussion of potential sources for the Fe enrichments in Arctic Ocean sediments. We also evaluate whether diagenetic processes influence the sedimentary Fe and Mn records in the same way.

105

106 2. Material and methods

107

108 During R/V *Polarstern* expeditions ARK-XXIII/3 in 2008 and ARK-XXVI/3 in 2011
109 (Jokat, 2009; Schauer, 2012), five gravity corer (GC) and eight multicorer (MUC)
110 cores were collected (Fig. 1, Table 1). Shortly after core recovery, the GC cores were
111 cut into 1 m segments. Pore water sampling was performed immediately with rhizons
112 (polymer filter with 0.1 µm pore size, Rhizosphere; Seeberg-Elverfeldt et al., 2005) at
113 4°C. Every 20 cm, holes were drilled into the liners of the GC cores. The rhizons
114 were placed into the holes and syringes were attached. Pore water sampling of the
115 MUC cores was performed in the same way on pre-drilled holes of the MUC tube (1-
116 5 cm intervals). Variable amounts of pore water were retrieved (5-10 ml) and stored
117 at 4°C in polypropylene tubes. For later analyses of dissolved metals the pore water
118 was acidified with distilled HNO_3 to a pH of <2. Pore water for nutrient analyses was
119 preserved by addition of $HgCl_2$. Sediment samples were taken with a plastic spatula
120 at a resolution of 1-5 cm and stored in plastic bags at 4°C. Sediments from all MUC
121 cores and one GC core (248-6) were taken on board. For later on-shore sampling of
122 GC cores 206-3, 220-7, and 237-3, plastic U-channels were used. After freeze-drying
123 at the University of Oldenburg, the samples were finely ground (< 0.125 mm) in an
124 agate ball mill for further analyses.
125 Analysis of pore water ammonia was performed on board with the untreated pore
126 water via photometry using a microtiter plate reader (Spectra Tecan; modified
127 protocol based on Benesch and Mangelsdorf, 1972). Nitrate was analyzed on shore
128 with a microtiter plate reader as well (Multiskan Go, Thermo Scientific; Schnetger and
129 Lehners, 2014). Dissolved Mn (Mn_{diss}) and S (calculated as SO_4^{2-}) were analyzed by
130 inductively coupled plasma-optical emission spectrometry (ICP-OES, Thermo-Fisher

131 iCAP 6000). Dissolved Co, Fe, and Mo (Co_{diss}, Fe_{diss}, Mo_{diss}) were analyzed in
132 medium resolution (4500) by ICP-mass spectrometry (Element 2, Thermo-Finnigan)
133 with Lu and Y as internal standards. Sediment analyses of Al, Co, Fe, Mn, Mo, and
134 Ni were performed by wavelength-dispersive X-ray fluorescence (XRF, Philips PW
135 2400) on fused borate glass beads (detailed method in data repository of Eckert et al.,
136 2013). For ICP-OES analyses, accuracy and precision were determined with the
137 standard NASS-5 (n = 7) and Mn-spiked Atlantic Sea Water (n = 23), and were <5%.
138 For ICP-MS analyses, accuracy and precision were monitored with the standard
139 CASS-5 (n = 10) and were <8% for Fe (accuracy only), Co, and Mo. Precision of Fe
140 measurements was 27%, likely due to sample concentrations close to the detection
141 limit. Several in-house standards (CAST, ICBM-B, Loess, PS-S, Peru) were used to
142 determine accuracy and precision for XRF measurements, which were <4% for major
143 elements and <9% for trace elements.
144 The water content of each sample, determined as the difference between wet and
145 freeze-dried sediment weight, was used to calculate the content of each sea salt
146 constituent. All data were then salt-corrected to eliminate dilution effects resulting
147 from sea salt enclosed in interstitial waters. Element contents are displayed in
148 weight-% for major elements or ppm (µg/g) for trace elements, and are normalized to
149 Al (according to Meinhardt et al., 2014). Average shale (AS; Wedepohl, 1971, 1991),
150 which represents the mean composition of weathered upper continental crust, was
151 used as a reference value.
152 Element excess contents were calculated according to Brumsack (2006):
153
154 $$element_{xs} = element_{sample} - Al_{sample} \bullet (element/Al)_{min} \quad (1)$$
155

where $(element/Al)_{min}$ indicates the lowest ratio in the respective core to compare the authigenic enrichments of certain elements relative to the local terrigenous input.

For analyses of Fe isotope ratios at the University of Hannover, Germany, 100 mg of each sample were dissolved in a mixture of 1.5 ml distilled conc. HNO_3 and 7.5 ml conc. HF (Merck® Suprapure) in PFA vessels heated in a microwave (CEM Mars 5 Express; operated at 1200 W, 190°C, for 2 h). The clear solutions were transferred into Savillex® beakers and evaporated at ~100°C. To remove potential fluoride compounds, the samples were treated subsequently step-wise with distilled hot conc. HNO_3, aqua regia, and 6 M HCl overnight. Separation of Fe employed 1.8 ml AG1 X8 anion resin (100-200 mesh; Bio-Rad®) loaded into columns made of polypropylene (Bio-Rad®). Iron was separated quantitatively after a slightly modified protocol from Dauphas et al. (2009) by using 3 M HNO_3 instead of 0.4 M HCl for resin cleaning prior to column separation. The procedure was repeated to obtain a pure Fe fraction (see Mansfeldt et al., 2012). Concentrated distilled HNO_3 and H_2O_2 (30%, Merck® Suprapure) were added to remove potential organic compounds leached from the resin, and dried at 105°C. The dry Fe fraction was dissolved in 1 ml 3 M HNO_3. Measurements of Fe isotope ratios were carried out via high resolution-multi collector-ICP-MS (Neptune Plus, Thermo-Scientific; see e.g., Weyer and Schwieters, 2003). The sample solutions were diluted to yield 3% HNO_3 and ~7 ppm Fe. A Ni standard solution (NIST 986, National Institute of Standards and Technology, USA) was added to samples and standards for instrumental mass bias correction as outlined by Oeser et al. (2014). The signal intensity was ~20 V for ^{56}Fe and ~4 V for ^{60}Ni. The interference of ^{54}Cr on ^{54}Fe was corrected by measurement of ^{53}Cr. Analyses followed the standard-sample-standard bracketing method.

The results are given in the delta notation:

$$\delta^{56}Fe\ (‰) = [(^{56}Fe/^{54}Fe_{sample})/(^{56}Fe/^{54}Fe_{IRMM\text{-}14})] \cdot 10^3 \quad (2)$$

relative to the international Fe isotope standard IRMM-14 that was analyzed before and after each sample.

The average reproducibility (2 standard deviation, 2s.d.) of the measurements was ±0.05‰ for δ^{56}Fe, determined by triplicate analyses of each sample (Table 1). The reference materials SDO (Devonian shale) and BCR-2 (basalt), and the in-house standard Fe-ETH (a Fe salt from the ETH Zürich; see, e.g., Kiczka et al., 2011) were used to determine the analytical accuracy of the Fe separation procedure. Results for the SDO (δ^{56}Fe = 0.024‰, 2s.d. = ±0.05‰, n = 6), the BCR-2 (δ^{56}Fe = 0.107‰, 2s.d. = ±0.02‰, n = 3), and the Fe-ETH (δ^{56}Fe = -0.711‰, 2s.d. = ±0.06, n = 6) are in excellent agreement with reference values of 0.008-0.036‰ for SDO, 0.022-0.098‰ for BCR-2 (GeoRem, see references), and -0.71‰ for Fe-ETH (e.g., Kiczka et al., 2011; Fehr et al., 2008).

3. Results

3.1 Preliminary stratigraphy

An age model for the studied sediment cores has not been published so far but there are prominent sediment features that may serve as stratigraphic marker horizons. Here we refer to distinct, wide-spread dark gray sediment layers which occur in different parts of the Arctic Ocean (Jakobsson et al., 2000; Löwemark et al., 2014). They are mostly centimeters to meters thick and interpreted as diamicts synchronously deposited by either freshwater discharges from Eurasian ice-dammed

lakes (Spielhagen et al., 2004) or the release of large quantities of icebergs from the extended Barents-Kara ice sheet (Jakobsson et al., 2014). Two distinct gray diamicts have been identified in the upper meters of several sediment cores from the Lomonosov Ridge (Fig. 2). They are characterized by generally lower Mn concentrations and elevated total organic carbon (TOC) concentrations. However, these characteristics may vary within the diamicts (Löwemark et al., 2014). In core 248-6 from the Lomonosov Ridge, two distinct dark gray sediment layers are located at ~220 cm and ~480 cm depth, and we tentatively assign them to MIS 4/3 (Jakobsson et al., 2001; Löwemark et al., 2012) and MIS 6 (Löwemark et al., 2012; 2014), respectively (Fig. 2). There are some other layers in the sediment core with mixed grayish/brownish color, but for our age correlation we only refer to distinct very dark gray layers of more than 1 cm thickness.

3.2. Sedimentary characteristics

Core 248-6 is mostly composed of alternating dark brown and olive brown sediment layers. The dark brown layers generally have elevated ratios of Mn/Al, Fe/Al, Co/Al, Mo/Al, and Ni/Al (Fig. 3), which is in accordance with previous geochemical studies in Arctic Ocean sediment cores (März et al., 2011; Meinhardt et al., 2014). These elevated values demonstrate scavenging of Mn/Fe (oxyhydr)oxides and associated trace metals from the water column (Goldberg, 1954; Bertine and Turekian, 1973). Olive brown sediment layers usually have lower ratios of these elements. The dark brown layers are partly enriched in other elements such as As, Cu, and V (not shown), but in this study we focus on Co, Mo, and Ni. Between 430 and 470 cm depth, mm-thick, closely spaced (mm to cm) layers appear dark in the core but white (i.e., with a high density) in the x-ray radiographs (Fig. 4). The spacing of discrete

XRF samples is too low to resolve these layers individually but the respective sediment interval is overall enriched in Mn, Co, and Mo, especially above 465 cm (Figs. 3, 4). Some of the dense layers show dendritic, “frosted” structures in the x-ray radiograph (455 and 460 cm, Fig. 4).

Core 206-3 from the Gakkel Ridge has only one dark brown sediment layer at ~250 cm depth and three dark gray sediment layers (Fig. 5). In contrast to core 248-6, the dark brown layer in core 206-3 is not enriched in Mn, Co, Mo, or Ni.

Core 220-7 from the Lomonosov Ridge near the North Pole has four dark brown sediment layers enriched in Mn, Co, Mo, and Ni. Two of the layers are also enriched in Fe (Fig. 6).

In core 237-3 from the Canada Basin, enrichment patterns of sedimentary Mn and trace metals in the dark brown sediment layers are very similar to core 248-6, whereas the ratios of Fe/Al are almost constant plotting close to the average shale ratio (Fig. 7).

3.3 Pore water characteristics

In core 248-6, the NO_3^- concentration has a subsurface maximum of 23 µM at ~30 cm (Fig. 3), resulting from O_2 reduction (Emerson et al., 1980). The NO_3^- concentrations reach the detection limit at ~5 m depth, following an approximately linear concentration gradient down to ~4 m depth. Below ~4 m depth NH_4^+ concentrations start to increase to the bottom of the core. Similar to NH_4^+, the Mn_{diss} concentration increases downcore from below detection limit at ~4 m depth to 120 µM at the bottom of the core. The SO_4^{2-} concentration is approximately constant. Pore water Mn_{diss} increases concomitantly with Co_{diss} and Mo_{diss}. The Co_{diss} profile shows a sharp peak, whereas the Mo_{diss} profile increases smoothly from around the

Arctic seawater value (Tovar-Sánchez et al., 2010) downcore to higher concentrations.

In contrast to Mn, dissolved Fe is mostly below the quantification limit in core 248-6, except for one sample where dissolved Fe is slightly increased (Fig. 3).

Pore water characteristics of core 206-3 are similar to core 248-6, with NO_3^- decreasing from the sediment-water interface to ~1 m depth, only very slightly decreasing SO_4^{2-} concentrations, and broad maxima in Mn_{diss} and Co_{diss} (Fig. 5). Pore water concentrations of Co_{diss} are comparable to core 248-6, but Mn_{diss} concentrations are ten times lower, and Mo_{diss} concentrations range around the seawater value without any indication of Mo_{diss} release into the pore waters.

In core 220-7 the profiles of NO_3^-, SO_4^{2-}, and Mn_{diss} are similar to core 206-3 (Fig. 6). A narrow maximum for Co_{diss} is recorded in the upper part of the Mn reduction zone. The Mo_{diss} profile is similar to the Mn_{diss} profile, but broader with a deeper enrichment. Fe_{diss} is below detection limit.

The pore water data of core 237-3 are different compared to the other three cores (Fig. 7). Nitrate only slightly increases downcore. Ammonia, Mn_{diss}, Fe_{diss}, and Co_{diss} are mostly below quantification limit. There is neither a decrease in SO_4^{2-} nor an increase in Mo_{diss} with depth.

3.4 Sedimentary Fe enrichments

3.4.1 Iron budget

To assess the potential origin of the Fe enrichments in the studied sediments, we performed an iron budget for the Arctic Ocean (Table 2). Based on the approach of Macdonald and Gobeil (2012), we used the input and output rates of water and

sediment, literature values for the concentrations of the different parameters in Table 2, and our own sediment data. Particulate matter was partitioned into lithogenic (Fe_{Lith}) and non-lithogenic (Fe_{NL}) fractions. The lithogenic component represents Fe that is incorporated into the mineral matrix and does not participate in redox reactions. The non-lithogenic component may be mobilized by redox reactions either within sediments of the continental shelf or within sediments in the deep ocean. This fraction is of interest in terms of possible diagenetic modification in the sedimentary record. To determine Fe_{Lith} and Fe_{NL}, we used data for shelf sediments from Strekopytov (2003). For simplification, we calculated the average Fe_{xs} in these cores, which we regard as Fe_{NL} (1.14%). Subtracting this value from the total Fe results in an average Fe_{Lith} of 4.78%. The ratio of Fe_{Lith}/ Fe_{NL} is 80/20, therefore 80% of a parameter in Table 2 accounts for the lithogenic component, and 20% for the non-lithogenic component.

Input and output rates of water and sediment per year from Macdonald and Gobeil (2012) were used to calculate the different Fe amounts per year for the parameters (see Table 2).

Hydrothermal activity in the Arctic Ocean has been observed at the ultraslow Gakkel Ridge spreading center (e.g., Edmonds et al., 2003). However, we can only estimate the amount of hydrothermal Fe because there are no direct measurements of material fluxes. For the Pacific and Atlantic outflows we used the same concentrations as for the inflows. Particulate matter from ice and sediment export is thought to have the same concentration as material from coastal erosion.

The input/output ratios of lithogenic, non-lithogenic, and total Fe in Table 2 are 0.86, 0.90, and 0.87, respectively. According to these numbers, 10-15% of the Fe inventory is exported from the Arctic Ocean. Because the output term includes deposition in shelf and basin sediments, it is likely that these 10-15% are

312 accumulated in the sediments, rather than being exported completely from the Arctic
313 Ocean.
314
315 3.4.2 Iron isotope ratios
316
317 We determined δ^{56}Fe values in 26 samples from eight different coring sites across
318 the central Arctic Ocean, including seven surface sediment samples, nine samples
319 from brown layers, three samples from gray layers, and seven background sediment
320 samples (Fig. 1, Table 1). Overall, the δ^{56}Fe values in all studied samples range
321 from -0.22 to +0.27‰ (Fig. 8, Table 1). Dark brown sediment layers show only
322 slightly lower δ^{56}Fe values (0.045 on average) than olive brown layers (0.056 on
323 average). The gray layers of cores 206-3 and 248-6 have higher δ^{56}Fe values
324 ranging from 0.17 to 0.27‰. These gray layers have very low Fe and Mn contents
325 (Figs. 3, 5) and very high ratios of Fe_{Lith}/Fe_{NL} (from 27 to 125; Table 1), implying that
326 the Fe pool is dominated by terrigenous, non-reactive Fe. All samples show a clear
327 negative relationship between their Fe/Al and δ^{56}Fe values (Fig. 9, data in Table 1).
328
329 4. Discussion
330
331 4.1 Potential origin of the Mn enrichment in core 248-6
332
333 Coastal erosion and river input are considered to be the two dominant sources for
334 non-lithogenic Mn in the open Arctic Ocean today (Macdonald and Gobeil, 2012),
335 with an intermittent diagenetic shuttling mechanism across the shelves (Löwemark et
336 al., 2014). It is currently unknown if Mn inputs for the Arctic Ocean were different in
337 the geological past, or if the values from Macdonald and Gobeil (2012) can be

338 applied to calculate past Arctic Mn budgets as well. We approach this question by
339 calculating the cumulative excess Mn (ar_{Mn248}) in the open marine core 248-6 from
340 the sediment surface to 480 cm depth (dark gray layer tentatively attributed to MIS 6
341 in Fig. 2, with an age of ~135,000 years). This excess Mn is compared with the
342 amount that could have been derived exclusively from river input, coastal erosion,
343 and additional sources like hydrothermal or eolian input ($ar_{MnInput}$; see details in the
344 Appendix (1.), (2.), and Table 3). The resulting average Mn accumulation rate in core
345 248-6 over the last 135,000 years (0 to 480 cm sediment depth) is $ar_{Mn248} = 1.6 \cdot 10^{-5}$
346 g cm^{-2} a^{-1}.
347 The Mn accumulation for the Arctic basins and submarine ridges under current input
348 conditions amounts to $ar_{MnInput} = 0.81 \cdot 10^{-5}$ g cm^{-2} a^{-1}. This value explains only 50%
349 of the ar_{Mn248}.
350 Three different processes may have affected this high Mn accumulation in core 248-6:
351 1) The coastal erosion and river Mn input fluxes determined by Macdonald and
352 Gobeil (2012) for the modern Arctic Ocean were much higher in the past, especially
353 during deglacial sea level rises when coastal erosion and the hydrological cycle were
354 strongly intensified.
355 2) The studied core 248-6 is not representative, i.e., it received a significantly higher
356 input of non-lithogenic Mn than the “average” Arctic basin and submarine ridge
357 environments. Indeed, in three other cores from different parts of the Arctic Ocean
358 (Lomonosov Ridge, Gakkel Ridge; Fig. 1, Table 3), 100% of Mn_{xs} in sediments
359 younger than MIS 6 can be explained by non-lithogenic input fluxes according to
360 Macdonald and Gobeil (2012). Overall, in three of four selected cores, the modern
361 non-lithogenic Mn input is sufficient to explain cumulative Mn_{xs} contents over the last
362 ~135,000 years, supporting the validity of the modern Arctic Mn budget at least for
363 the last glacial cycle.

3) A significant fraction of non-lithogenic Mn in the sediment interval from 0 to 480 cm depth in core 248-6 is derived from deeper sediment layers where it was released during diagenesis. This latter explanation is supported by the pore water profiles (Fig. 3) and specific sediment structures (Fig. 4), as will be discussed in the following sections.

4.2 Diagenetic trace metal cycling in core 248-6

Pore water composition can provide valuable information on the contribution of diagenetic processes to sediment geochemistry. Microbially mediated redox reactions usually alter the sediment composition after deposition by following the catabolic sequence of electron acceptors during microbial degradation of organic matter: O_2, NO_3^-, Mn (oxyhydr)oxides, Fe (oxyhydr)oxides, SO_4^{2-} and CH_4 (Froelich et al., 1979). The activation of a specific electron acceptor in a sediment succession depends on its availability, the energy gain of the reaction, and the microbial community present in the sediments. These electron acceptors (e.g., NO_3^-, SO_4^{2-}) or their metabolic products (e.g., Mn^{2+}, Fe^{2+}, NH_4^+) can be detected and analyzed in the pore waters.

The presence of NH_4^+ in core 248-6 (Fig. 3) indicates the absence of O_2. In the presence of O_2 NH_4^+ would be oxidized to NO_3^-. Oxygen may be present down to ~4 m depth, but direct measurements were not performed. Pore water Mn_{diss} concentrations are most likely induced by dissimilatory Mn reduction below ~4 m depth (Froelich et al., 1979). Sulfate-reduction does not seem to play a major role in the upper 6 m of this core.

Collectively, the pore water profiles of core 248-6 imply that:

1) NO_3^- has a very deep sediment penetration depth of ~5 m,

390 2) dissimilatory Mn^{IV} reduction below ~5 m depth is likely an important pathway of
391 organic matter re-mineralization whereas NH_4^+ may diffuse upward from deeper
392 layers with ongoing SO_4^{2-} reduction (Backman et al., 2006),
393 3) the top of the Mn^{IV} reduction zone is determined by the NO_3^- penetration depth.
394 Compared to other parts of the global ocean, NO_3^- pore water measurements from
395 the Arctic Ocean are rare. Hulth et al. (1996) calculated a NO_3^- penetration depth of
396 up to 8 cm in marine sediments around Svalbard. Concentrations of NO_3^- in pore
397 waters from giant box corer sediments (max. 50 cm depth) from the Kara Sea
398 indicate NO_3^- reduction at these depths as well (Damm, 1999).
399 One sample with elevated Fe_{diss} concentration value (Fig. 3) does not necessarily
400 show a recent significant pore water Fe flux that may influence the solid phase Fe
401 distribution, and is therefore considered an outlier. In the sediment interval below the
402 NO_3^- reduction zone, the redox potential seems to be sufficiently low for
403 Mn(oxyhydr(oxide) reduction, but still too high for significant Fe(oxyhydr(oxide)
404 reduction.
405 Regarding diagenetic Mn redistribution within the sediments, it seems evident that a
406 Mn_{diss} sink is located just below 4 m depth in core 248-6 (Fig. 3). The source of Mn_{diss}
407 must be located at the bottom of the core or below. At ~460 cm, where Mn_{diss}
408 concentrations start to increase, a peak in sedimentary Mn/Al is observed, most likely
409 caused by precipitation of Mn (oxyhydr)oxides at the Mn redox boundary upon
410 contact with nitrate or possibly oxygen (Lovley and Phillips, 1988; Hulth et al., 1999),
411 as suggested by März et al. (2011). Pore water Mn_{diss} may precipitate at or adsorb on
412 existing (oxyhydr)oxide surfaces (Murray, 1975), or form new authigenic Mn
413 (oxyhydr)oxides (Li et al., 1969; Burdige 1993).
414 The occurrence of dendritic structures in the x-ray radiographs has been reported in
415 another sediment core from the Lomonosov Ridge by Löwemark et al. (2012), and is

explained to represent purely authigenic Mn precipitates (see also März et al., 2011; Löwemark et al., 2014). The thin dendritic layers have a dark brown sediment color (Fig. 4), which indicates that they may consist of Mn oxides. Mobilization of Mn_{diss} from deeper sediment layers and reprecipitation at the Mn redox boundary may form these layers under steady-state conditions. The depth interval at which these layers form depends on oxygen penetration, which in turn depends on organic matter availability and sedimentation rate.

Co and Mo seem to be diagenetically recycled along with Mn (Fig. 3; see Tribovillard et al., 2006, for background on Co and Mo redox chemistry). This process of Co and Mo release into, and removal from, pore waters in close association with the diagenetic Mn cycle, has been described in other oxic settings (e.g., Knauer et al., 1982; Gendron et al., 1986; Shaw et al., 1990; Morford and Emerson, 1999). The proposed dissolution-reprecipitation process is in agreement with our pore water data: Both Mn_{diss} and Co_{diss}, which show elevated concentrations near the core bottom, decrease to minimum concentrations in the sediment interval around 460 cm depth, indicating precipitation of these elements within this interval (Fig. 3). Interestingly, Mo_{diss} requires a much longer diffusion pathway than Mn and Co to reach background concentrations, possibly because the sedimentary Mn surfaces are saturated with Mo.

Based on pore water and sedimentological patterns in core 248-6, we conclude that the brown layer at ~445-470 cm depth has experienced, and still is experiencing, diagenetic addition of Mn, Co, and Mo. To further evaluate if these diagenetic additions have impacted the sediment geochemistry in a particular way, we compare the fractions of the excess contents of Mn, Co, and Mo in this brown layer with each other. Differences in the behavior of these specific trace metals during Mn diagenesis in the Arctic were first reported for sediments from the Mendeleev Ridge by März et

al. (2011). They proposed the use of Co/Mo values to distinguish between authigenic and diagenetic Mn layers. Higher Co/Mo in layers indicate diagenetic loss of Mn and Mo from the solid phase, and lower Co/Mo indicate post-depositional addition of Mn and Mo. Their results are in accordance with the results in Fig. 10a, where Co_{xs}/Mo_{xs} values of all Mn-enriched layers in core 248-6 are illustrated. The highest ratios of >=10 are found in those layers located in the Mn and Mo reduction zone deeper than 500 cm, whereas lowest ratios of <=1 are found in the layer at ~460 cm depth with diagenetic Mo addition, supporting the findings of März et al. (2011). Samples with Co_{xs}/Mo_{xs} >1 and <10 are considered to be primary layers. Considering Co_{xs}/Mo_{xs} values is therefore a promising tool for the identification of diagenetically overprinted sediment intervals when pore water data are missing. The basis for using this proxy is the different behavior of Co and Mo during diagenesis. In Mn-rich layers Mo and Co are adsorbed to the surface of Mn oxides. During partial dissolution of these layers Mo is preferentially released to the pore water compared to Co, because Co has a high specific adsorption potential to MnO_2 surfaces (Murray, 1975; Murray and Dillard, 1979). The reduced Mn_{diss} can partly re-adsorb on the remaining Mn oxides whereas Mo_{diss} remains in solution (Shimmield and Price, 1986). Therefore Co remains preferentially in the sediment layers, whereas Mo and Mn are released to the pore water. Similar observations were reported by März et al. (2011).

4.3 Pore water flux calculation and Mn_{diss} reduction rate for core 248-6

We have previously concluded that at site 248-6 around 50% of the excess Mn accumulating over the past ~135,000 years (0-480 cm sediment depth) cannot exclusively be explained by external sources (Macdonald and Gobeil, 2012). The brown layer at ~445-470 cm is gaining Mn, Co, and Mo diagenetically. The question

arises if the current pore water fluxes of Mn, Co, and Mo, into the brown layer at ~445-470 cm could have generated the observed post-depositional element enrichments. Therefore we performed simple pore water flux calculations (assuming steady state conditions) based on Fick's first law of diffusion (Schulz, 2006), following an approach by März et al. (2011; 2015; see Table 4, Appendix (3.)):

The resulting diffusive pore water flux J_{sedMn} is $-0.59 \cdot 10^{-3}$ mol m^{-2} a^{-1}. The calculated burial pore water flux is three orders of magnitude lower and can be disregarded (Appendix (4.)).

The sediment layer at ~445-470 cm depth has a tentative age of ~120,000 years (located above the MIS 6 deposit), which is the maximum time that might have been available for diagenetic Mn enrichment. Assuming that the pore water flux was stable for the last 120,000 years, 13.5 g kg^{-1} Mn_{xs} could have been produced by this flux (Appendix (5.); Table 4). However, the average Mn_{xs} content of the respective interval is only 9.1 g kg^{-1}, which implies that the current Mn flux into this sediment layer was only established significantly after its deposition. Under steady-state conditions, it would have taken at least ~80,000 years to accumulate the measured Mn_{xs} content (Appendix (6.)). Even if the current Mn flux was only established at the onset of the Holocene (~12,000 years BC), it could still have contributed up to ~15% of the total Mn_{xs} inventory between 445 and 470 cm depth at site 248-6 (Appendix (7.); Table 4).

Pore water fluxes for Co and Mo were calculated as well, analogous to the calculations for Mn (Table 4). Cobalt and Mo pore water fluxes are three orders of magnitude lower than for Mn, which is in accordance with the pore water concentrations of Co_{diss} and Mo_{diss}. After 80,000 years at steady-state conditions, the current pore water fluxes of Co and Mo can explain 61% and >100% of the sedimentary Co and Mo enrichments in the sediment layer between 445 and 470 cm, respectively (Table 4). After 12,000 years, 9% of the Co enrichment and 45% of the

494 Mo enrichment can still be explained by the pore water flux. The Co addition from the
495 pore water flux is similar to that of Mn, whereas Mo is marked by an elevated
496 diagenetic addition. These simple steady-state calculations only provide relatively
497 rough estimates of the potential diagenetic Mn (as well as Co and Mo) contribution to
498 a specific brown sediment layer, and more advanced reaction-transport modelling
499 simulating non-steady state conditions would be required to better constrain these
500 values. However, our data still confirm recent studies of relatively fast diagenetic Mn
501 redistribution in open Arctic Ocean sediments (Sundby et al., 2015). We therefore
502 recommend that Mn layers within the Mn reduction or precipitation zone in Arctic
503 sediments should only be used with caution for correlation purposes, as they may
504 have lost or gained significant quantities of Mn_{xs} by diagenesis, respectively.
505 To further constrain rates of Mn_{diss} release into, and precipitation from the pore
506 waters at site 248-6, we applied the REC (Rate Estimation from Concentrations)
507 model from Lettmann et al. (2012, Fig. 11). For this model, we used the pore water
508 Mn_{diss} concentrations, porosity Φ (estimated from Stein et al., 2004), diffusion
509 coefficient D_{sed}, and sedimentation rate sr. The bioturbation coefficient D_b and the
510 bioirrigation factor were set to zero. In the interval above ~400 cm, net rates are
511 around zero, implying neither consumption nor production of Mn_{diss}. The rate is
512 negative in the interval from ~400 to 480 cm, implying consumption of Mn_{diss}, i.e.,
513 precipitation from the pore water. Below 480 cm depth, positive values indicate the
514 production of Mn_{diss}. The most negative rate values in the dark brown layer at ~460
515 cm depth are indicative of an enhanced Mn oxide precipitation in this layer.
516
517 4.4 Diagenetic conditions in sediment cores from different parts of the central Arctic
518 Ocean
519

Having studied and discussed core 248-6 from the Lomonosov Ridge in detail, we now compare diagenetic conditions and processes at this site with other parts of the Arctic Ocean, including the Gakkel Ridge (core 206-3), the Lomonosov Ridge near the North Pole (core 220-7), and the Canada Basin (core 237-3).

The fact that the dark brown layer in core 206-3 is not enriched in Mn, Co, Mo, or Ni implies that the color may rather result from higher Fe oxide contents, as indicated by higher Fe/Al (Fig. 5). The Mn redox boundary (~1 m) is located closer to the sediment/water interface compared to core 248-6 (~4.5 m), and again seems to be related to the NO_3^- penetration depth. Both, the sediment interval at ~350 cm depth without brown coloration and the brown layer at ~250 cm depth, have elevated Co_{xs}/Mo_{xs}, indicating loss of Mn (Fig. 10b). As the pore water Mn_{diss} starts to increase at ~350 cm depth and Mn/Al is elevated here (Fig. 5), this interval seems to be the source for dissolved Mn. In contrast, the Mn-rich interval from 38 to 45 cm, where the pore water gradient ends, has lower Co_{xs}/Mo_{xs}, comparable to the diagenetically influenced dark brown layer at 460 cm in core 248-6 (Fig. 10a). This indicates that despite the lack of dark brown coloration, diagenetic Mn and Mo addition from the pore waters likely influenced this Mn- and Mo-rich interval in core 206-3. Interestingly, pore water data (Fig. 5) show no current flux of Mo_{diss} into this sediment layer, so it can be assumed that the precipitation of remobilized Mo_{diss} at this site has occurred in the past. Overall, Mn and Mo remobilization seem to be less pronounced in this core. This may be due to the fact that sedimentary Mn (oxyhydr)oxide contents are lower as well, implying that the sparse availability of Mn^{IV} as an electron acceptor in combination with low organic matter contents limits the degree of Mn diagenesis. There is no systematic increase in pore water Fe_{diss} concentration in this core, indicating that significant diagenetic Fe^{III} reduction does not occur either.

545 The pore water gradients of Mn_{diss}, Co_{diss}, and Mo_{diss} in cores 206-3 and 220-7 do not
546 terminate in distinct brown layers (as they do in core 248-6), therefore pore water flux
547 calculations were not performed. However, in core 220-7 Co_{xs}/Mo_{xs} values are very
548 low (~1) in the interval from 90 to 100 cm depth where the pore water gradient ends,
549 and thus indicate diagenetic addition of Mo from the pore water pool (Fig. 10c). In
550 addition, Mn/Al is slightly increased above this interval. The Co_{xs}/Mo_{xs} values of the
551 brown layers show that the first one (at ~50 cm depth) is of primary origin, and that
552 the two layers at 160 cm and 260 cm experienced diagenetic loss of Mn. The
553 lowermost brown layer has elevated Mn/Al and Mo/Al and intermediate Co_{xs}/Mo_{xs},
554 which indicates that this layer is currently not influenced by diagenesis.
555 In core 237-3, Mn oxides with adsorbed Co, Mo, and Ni clearly seem to be
556 responsible for the dark brown color (Fig. 7). Nitrate, Mn^{IV}, and possibly O_2 are
557 available as electron acceptors, and it seems very likely that the low availability of
558 reactive organic matter is limiting diagenesis at this distal site in the Canada Basin.
559 The ratios of Co_{xs}/Mo_{xs} (Fig. 10d) of the brown layers are mostly between 1 and 10,
560 and suggest that the Mn-rich layers in this core are primary, which is in agreement
561 with the pore water profiles (Fig. 7). The topmost samples have higher Co_{xs}/Mo_{xs},
562 which would indicate diagenetic loss, but the pore water concentrations of Mn_{diss} are
563 below detection limit in the upper centimeters. These data show that the sediment
564 geochemistry of Mn, Fe, Co, and Mo in core 237-3 is presently not overprinted by
565 diagenetic processes.
566 In summary, the observations described above demonstrate the occurrence of
567 different diagenetic regimes in different parts of the central Arctic Ocean:
568 1) Core 237-3 from the Canada Basin does not show any signs of current Mn, Fe, Co,
569 and Mo diagenesis.

570 2) Core 248-6 from the Lomonosov Ridge is diagenetically influenced by Mn
571 reduction and associated Co and Mo cycling, which in part affects a dark brown
572 sediment layer at ~460 cm depth. In core 220-7 from the Lomonosov Ridge, close to
573 the North Pole, pore water data indicate Mn, Co, and Mo remobilization as well, but
574 possible effects on specific dark brown layers could not be quantified.
575 3) Core 206-3 from the Gakkel Ridge is clearly influenced by Mn reduction and
576 additional Co remobilization.
577 The data also show that Co and Mo are not remobilized in the same way during the
578 dissolution of Mn layers in different parts of the Arctic Ocean. In core 248-6 pore
579 water data indicate that Mn and Co are removed from the pore water in one specific
580 sediment layer, while Mo seems to precipitate in the overlying sediment as well (Fig.
581 3). In core 220-7, on the other hand, both Mn and Mo seem to precipitate in the same
582 sediment layer (Fig. 6). In all cores Mn diagenesis is evidently controlled by the NO_3^-
583 penetration depth. The absence of diagenetic overprint of core 237-3 might be
584 related to its distal position in the Canada Basin and the greater water depth
585 compared to the other cores (Table 1).
586 Based on these geochemical pore water and sediment data, we conclude that,
587 despite some discrepancies in Co and Mo remobilization into the pore waters,
588 Co_{xs}/Mo_{xs} values are indeed indicative of diagenetic overprint of Mn-rich sediment
589 layers in most of the studied sediment cores from the Arctic Ocean.
590
591 4.5 Sedimentary Fe enrichments
592
593 Our pore water data show that Fe diagenesis is negligible in all studied cores.
594 Therefore the question arises whether Fe enrichment patterns could be used as
595 diagenetically stable tracers for elevated metal inputs into the Arctic Ocean, as

596 already proposed by März et al. (2012). Iron isotopic signatures could additionally
597 provide information about different sources of metals to the Arctic Ocean (including
598 coastal erosion, river input, hydrothermal input). These hypotheses are explored in
599 the following section.
600 A comparison of the Fe accumulation rate in core 248-6 with the input values from
601 our budget (Table 3) shows that the Fe enrichment in the core can easily be
602 explained by these external sources. In support of this, the pore water data (Fig. 3)
603 do not indicate any Fe addition from deeper sediment layers. In three other cores
604 (Table 3) the external sources are more than sufficient to account for the Fe
605 enrichment as well. We assume that the input parameters used by Macdonald and
606 Gobeil (2012) are only applicable to calculate the present Fe budget of the Arctic
607 Ocean. The Fe input might have been lower in the past during glacials due to the
608 presence of ice sheets and a lower sea level and might have fluctuated between
609 glacial and interglacial times. In the next step, we evaluate the Fe isotopic signature
610 of several sediment cores to distinguish between different lithogenic and non-
611 lithogenic Fe sources to the Arctic Ocean basins, and their variation over time.
612 The differences in δ^{56}Fe between dark brown and olive brown layers (Figs. 8, 9) are
613 within the standard deviation of the measurements and imply that different
614 environmental conditions during glacial and interglacial periods have only a minor
615 influence on the Fe isotopic fractionation in central Arctic Ocean sediments.
616 The geochemical patterns of the gray layers (Figs. 3, 5) either represent the residual
617 Fe fraction after dissolution and loss of more labile Fe minerals with lower δ^{56}Fe
618 values (e.g., during continental weathering; Fantle and DePaolo, 2004), or document
619 a different sediment provenance. The gray layers are depleted in Fe, but enriched in
620 the elements Si and Zr (not shown) that are usually associated with coarse-
621 grained/high-density detrital minerals (e.g., Calvert and Pedersen, 2007; März et al.,

622 2011). Therefore, these layers were most likely deposited under glacial conditions by
623 two possible scenarios (see chapter 3.1). During iceberg discharge events from the
624 Barents-Kara ice sheet, these icebergs would carry the specific isotopic signature
625 from the Barents-Kara hinterland. Unfortunately, δ^{56}Fe source rock data are not
626 available for the Arctic, but bulk granitoids, which represent a major fraction of
627 continental crustal rock material, have positive δ^{56}Fe values from ~0.1 to 0.4‰
628 (Poitrasson and Freydier, 2005). During the outburst of ice-dammed lakes, large
629 amounts of material were quickly deposited in the Arctic basins, shielding the
630 underlying sediment from the oxic water column. These gray layers have higher
631 organic matter contents than the surrounding sediments (Löwemark et al., 2014), and
632 therefore should provide fuel for diagenetic processes, including dissimilatory iron
633 reduction (DIR). During this process, isotopically light Fe is liberated to the pore
634 waters and diffuses out of this layer, leaving the residual sediment with a more
635 positive signature, and therefore a higher δ^{56}Fe (e.g., Crosby et al., 2005; 2007;
636 Johnson et al., 2008). The gray layers have very low Mo contents (often below
637 quantification limit), resulting in high Co_{xs}/Mo_{xs} values indicative for diagenetic loss of
638 Mn and possibly associated Fe. However, we can only infer that this diagenetic
639 process occurred in the past, as the present pore water profiles show no sign of
640 significant Fe reduction in the gray layers (Figs. 3, 5). We therefore define the gray
641 layers with the lowest Fe/Al and highest δ^{56}Fe values as the lithogenic background
642 for our sediment cores that has been largely deprived of its reactive, isotopically light
643 Fe fraction.
644 A negative Fe/Al to δ^{56}Fe relationship was also found in recent sediments from the
645 Black Sea (sub)oxic shelf and euxinic basin (Severmann et al., 2008; Eckert et al.,
646 2013). This pattern was attributed to the diagenetic loss of reactive, isotopically light
647 iron from suboxic shelf sediments via DIR, followed by shuttling of the remobilized Fe

pool across the basin, and its deposition in the euxinic deep water setting as isotopically light Fe sulphides. In contrast to the Black Sea, the constant pore water SO_4^{2-} concentrations and very low sedimentary S contents (close to the detection limit; not shown) in the studied Arctic Ocean sediments strongly argue against euxinic conditions and significant syngenetic or diagenetic pyrite formation. Evidence for this diagenetically driven shelf-to-basin Fe shuttle has also been found along other continental margins that are affected by upwelling of nutrient-rich waters and oxygen minimum zones (e.g., Homoky et al., 2012; Scholz et al., 2014), but the Arctic Ocean shelves and margins are not affected by oxygen-depleted water masses (Jakobsson et al., 2007; Stein 2008). Therefore, other biogeochemical and/or depositional processes must be invoked to explain the basin-wide negative Fe/Al to δ^{56}Fe relationship across all studied sediment cores.

Low δ^{56}Fe values indicate addition of an isotopically light Fe fraction to the sediment (Bergquist and Boyle 2006; Fehr et al., 2008; Severmann et al., 2008). Possible mechanisms for this addition include diagenetic mobilization by DIR or abiotic reduction by HS^- from underlying sediment layers (Berner, 1984; Beard et al., 1999; Haese et al., 2000; Brantley et al., 2004), or from the continental shelf (via a shuttle transport mechanism). Dissimilatory Fe reduction occurs in the organic-rich Arctic shelf sediments that often display non-lithogenic Fe (oxyhydr)oxide enrichments at the sediment surface (Turner and Harriss, 1970; Nolting et al., 1996; Hölemann et al., 1999; Strekopytov, 2003). An Fe shuttle in the well-oxygenated Arctic Ocean must have been different from Fe shuttling in oxygen minimum zones or anoxic zones as present in the Black Sea. Possible transport pathways include hypopycnal distribution of organically complexed riverine Fe in the fresh surface layer, resuspension of Fe particles on the shelf by currents, and transport of Fe particles by seasonal sea ice (e.g., Nakayama et al., 2011; Thuroczy et al., 2011; März et al.,

674 2012; Klunder et al., 2012). Samples with lower δ^{56}Fe values generally also have
675 higher Mn/Al values, which indicates a close association of Fe with Mn. Recently it
676 was shown that Fe may be released from labile Fe-Mn oxides during Mn reduction
677 and that this Fe has low δ^{56}Fe values, leaving the residual Fe with a higher isotopic
678 signature (Schuth et al., 2015).
679 Another explanation for the negative δ^{56}Fe values is an input of isotopically light Fe
680 from the water column, probably via hydrothermal fluids, continental runoff, oceanic
681 crust alteration and shelf pore fluids (Beard et al., 2003; Bergquist and Boyle 2006;
682 Severmann et al., 2006). Specifically core 206-3 is located at the ultra-low spreading
683 Gakkel Ridge (Edmonds et al., 2003) and might have received periodic input of
684 hydrothermal Fe. Additional studies are required to further discriminate between
685 specific transport pathways or different Fe sources to the sediment.
686
687 5. Conclusions
688
689 The dark brown color of specific sediment layers from the central Arctic Ocean is
690 related either to enhanced Mn (oxyhydr)oxide content, Fe (oxyhydr)oxide content, or
691 a combination of both. These layers are characterized by enhanced Mo, Co, and Ni
692 contents due to scavenging from the water column. Pore water measurements reveal
693 different diagenetic regimes in Arctic Ocean sediment cores, ranging from strong
694 reduction and diagenetic overprint of Mn, Co, and Mo to the absence of these
695 processes in deeper sediment layers. Pore water flux calculations show that the
696 sedimentary enrichments of Mn, Co, and Mo can be altered by a significant post-
697 depositional contribution from the current pore water flux. Ratios of Co_{xs}/Mo_{xs} of the
698 dark brown layers form a helpful proxy to identify sediment layers with diagenetic
699 addition from the pore water or diagenetic dissolution in the Mn reduction zone.

Sedimentary Fe enrichments are primarily derived from external input. The lithogenic Fe fraction accounts for 80% of the total Fe, only 20% is of non-lithogenic origin. Gray layers define the lithogenic background with low Fe/Al, high Fe_{Lith}/Fe_{NL}, and positive $\delta^{56}Fe$ values. With increasing Fe/Al the $\delta^{56}Fe$ values decrease. This indicates the presence of a dominant diagenetic Fe fraction with a low $\delta^{56}Fe$ signature. Pore water Fe data show that remobilization from deeper layers within the sediment can currently be excluded. Therefore the presence of lighter Fe isotopes is likely a result of Fe transport from the shelf to the basin due to dissimilatory Fe reduction on the shelves. The absence of large variations in $\delta^{56}Fe$ values between dark brown and lighter layers indicates that the different environmental conditions during glacial and interglacial times have a minor influence on the Fe isotopic fractionation in the studied Arctic Ocean sediments. Thus, sedimentary iron isotopes in combination with pore water data and modeling are a potential tool for the identification of different diagenetic remobilization processes and, together with sedimentary Mn, Co, and Mo data, different transport processes. We emphasize that combined studies of sediment and pore water geochemistry should be performed in order to identify possible diagenetic overprinting of primary sediment composition in the Arctic Ocean.

Acknowledgements

The authors would like to thank the master, crew, and shipboard scientists onboard R/V *Polarstern* during the ARK-XXII/3 and ARK-XXVI/3 expeditions, R. Stein for discussion and guidance in the preparation of the sampling plan, and E. Gründken, C. Lehners and M. Schulz for substantial analytical assistance. The comments of the editor and three anonymous reviewers helped to improve the manuscript. Helen

Talbot kindly improved the English language. This study was supported by the German Research Foundation (DFG grant BR 775/27-1) within the IODP SPP, which is gratefully acknowledged.

References

Aagaard K. and Swift J. H. (1985) Thermohaline Circulation in the Arctic Mediterranean Seas. J. Geophys. Res. **90**, 4833-4846.

Aguilar-Islas A. M., Hurst M. P., Buck K. N., Sohst B., Smith G. J., Lohan M. C. and Bruland K. W. (2007) Micro- and macronutrients in the southeastern Bering Sea: Insight into iron-replete and iron-depleted regimes. Prog. Oceanogr. **73**, 99-126.

Alexanderson H., Backman J., Cronin T. M., Funder S., Ingólfsson Ó., Jakobsson M., Landvik J. Y., Löwemark L., Mangerud J., März C., Möller P., O'Regan M. and Spielhagen R. F. (2014) An Arctic perspective on dating Mid-Late Pleistocene environmental history. Quaternary Sci. Rev. **92**, 9-31.

Anisimov O. A., Vaughan D. G., Callaghan T. V., Furgal C., Marchant H., Prowse T. D., Vilhjálmsson H., and Walsh J. E. (2007) Polar regions (Arctic and Antarctic). Climate Change 2007: Impacts, Adaptation and Vulnerability. Contribution of Working Group II to the Fourth Assessment Report of the Intergovernmental Panel on Climate Change, M. L. Parry, O. F. Canziani, J. P. Palutikof, P. J. van der Linden and C. E. Hanson, Eds., Cambridge University Press, Cambridge, 653-685.

751 Backman J., Jakobsson M., Lovlie R., Polyak L. and Febo L. A. (2004) Is the central
752 Arctic Ocean a sediment starved basin? Quaternary Sci. Rev. **23**, 1435-1454.
753
754 Backman J., Moran K., McInroy D. B., Mayer L. A. (2006) Sites M0001-M0004.
755 Proceedings of the Integrated Ocean Drilling Program 302.
756
757 Beard B. L., Johnson C. M., Cox L., Sun H., Nealson K. H. and Aguilar C. (1999) Iron
758 isotope biosignatures. Science **285**, 1889-1892.
759
760 Beard B. L., Johnson C. M., Von Damm K. L. and Poulson R. L. (2003) Iron isotope
761 constraints on Fe cycling and mass balance in oxygenated Earth oceans. Geology
762 **31**, 629-632.
763
764 Benesch R. and Mangelsdorf P. (1972) Eine Methode zur colorimetrischen
765 Bestimmung von Ammoniak in Meerwasser. Helgoland Mar. Res. **23**, 365-375.
766
767 Bergquist B. A. and Boyle E. A. (2006) Iron isotopes in the Amazon River system:
768 Weathering and transport signatures. Earth Planet. Sci. Lett. **248**, 54-68.
769
770 Berner R. A. (1984) Sedimentary pyrite formation - An update. Geochim.
771 Cosmochim. Acta **48**, 605-615.
772
773 Bertine K. K. and Turekian K. K. (1973) Molybdenum in Marine Deposits. Geochim.
774 Cosmochim. Acta **37**, 1415-1434.
775
776 Boudreau B. P. (1997) Diagenetic Models and Their Implementation. Modelling

777 Transport and Reactions in Aquatic Sediments. Springer Verlag Berlin Heidelberg.
778
779 Brantley S. L., Liermann L. J., Guynn R. L., Anbar A., Icopini G. A. and Barling J.
780 (2004) Fe isotopic fractionation during mineral dissolution with and without bacteria.
781 Geochim. Cosmochim. Acta **68**, 3189-3204.
782
783 Brumsack H.-J. (2006) The trace metal content of recent organic carbon-rich
784 sediments: Implications for Cretaceous black shale formation. Palaeogeogr.
785 Palaeocl. Palaeoeco. **232**, 344-361.
786
787 Burdige D. J. (1993) The Biogeochemistry of Manganese and Iron Reduction in
788 Marine Sediments. Earth-Sci. Rev. **35**, 249-284.
789
790 Calvert S. E. and Pedersen T. F. (2007) Elemental Proxies for Paleoclimatic and
791 Paleoceanographic Variability in Marine Sediments: Interpretation and Application.
792 In: Developments in Marine Geology, Vol. 1, Proxies in Late Cenozoic
793 Paleoceanography, pp. 567-644.
794
795 Crosby H. A., Johnson C. M., Roden E. E. and Beard B. L. (2005) Coupled Fe(II)-
796 Fe(III) electron and atom exchange as a mechanism for Fe isotope fractionation
797 during dissimilatory iron oxide reduction. Environ. Sci. Technol. **39**, 6698-6704.
798
799 Crosby H. A., Roden E. E., Johnson C. M. and Beard B. L. (2007) The mechanisms
800 of iron isotope fractionation produced during dissimilatory Fe(III) reduction by
801 Shewanella putrefaciens and Geobacter sulfurreducens. Geobiology **5**, 169-189.
802

Damm E. (1999) Manganese, iron, and nutrients in pore water profiles from the Ob and Yenisei estuaries (Kara Sea). In: Matthiessen J., Stepanets O. V., Stein R., Fütterer D. K. and Galimov E. M. (eds.), The Kara Sea Expedition of RV Akademik Boris Petrov 1997: First Results of a Joint Russian-German Pilot Study, Rep. Polar Res., Alfred Wegener Institute for Polar and Marine Research, Bremerhaven, 300, 127-130, hdl:10013/epic.10303.d001

Dauphas N., Pourmand A. and Teng F. Z. (2009) Routine isotopic analysis of iron by HR-MC-ICPMS: How precise and how accurate? Chem. Geol. **267**, 175-184.

Duce R. A. and Tindale N. W. (1991) Atmospheric Transport of Iron and Its Deposition in the Ocean. Limnol. Oceanogr. **36**, 1715-1726.

Eckert S., Brumsack H.-J., Severmann S., Schnetger B., März C. and Fröllje H. (2013) Establishment of euxinic conditions in the Holocene Black Sea. Geology **41**, 431-434.

Edmonds H. N., Michael P. J., Baker E. T., Connelly D. P., Snow J. E., Langmuir C. H., Dick H. J. B., Muhe R., German C. R., and Graham D. W. (2003) Discovery of abundant hydrothermal venting on the ultraslow-spreading Gakkel ridge in the Arctic. Nature **421**, 252-256.

Emerson S., Jahnke R., Bender M., Froelich P., Klinkhammer G., Bowser C. and Setlock G. (1980) Early Diagenesis in Sediments from the Eastern Equatorial Pacific .1. Pore Water Nutrient and Carbonate Results. Earth Planet. Sci. Lett. **49**, 57-80.

829 Expedition 302 Scientists (2006) Moisture and density measured on Hole 302-
830 M0004C. doi:10.1594/PANGAEA.326708.
831
832 Fantle M. S. and DePaolo D. J. (2004) Iron isotopic fractionation during continental
833 weathering. Earth Planet. Sci. Lett. **228**, 547-562.
834
835 Fehr M. A., Andersson P. S., Halenius U. and Morth C. M. (2008) Iron isotope
836 variations in Holocene sediments of the Gotland Deep, Baltic Sea. Geochim.
837 Cosmochim. Acta **72**, 807-826.
838
839 Froelich P. N., Klinkhammer G. P., Bender M. L., Luedtke N. A., Heath G. R., Cullen
840 D., Dauphin P., Hammond D., Hartman B. and Maynard V. (1979) Early Oxidation of
841 Organic-Matter in Pelagic Sediments of the Eastern Equatorial Atlantic - Suboxic
842 Diagenesis. Geochim. Cosmochim. Acta **43**, 1075-1090.
843
844 Gaillardet J., Dupre B. and Allegre C. J. (1999) Geochemistry of large river
845 suspended sediments: Silicate weathering or recycling tracer? Geochim.
846 Cosmochim. Acta **63**, 4037-4051.
847
848 Gendron A., Silverberg N., Sundby B. and Lebel J. (1986) Early Diagenesis of
849 Cadmium and Cobalt in Sediments of the Laurentian Trough. Geochim. Cosmochim.
850 Acta **50**, 741-747.
851
852 GeoRem database reference values for BCR-2: http://georem.mpch-
853 mainz.gwdg.de/single_values_detail.asp?itemmeas=d56Fe&refmatid=USGS%20BC
854 R-2 (accessed June 23, 2015)

855

856 Goldberg E. D. (1954) Marine Geochemistry 1. Chemical Scavengers of the Sea. J.
857 Geol. **62**, 249-265.
858
859 Gordeev V. V., Rachold V. and Vlasova I. E. (2004) Geochemical behaviour of major
860 and trace elements in suspended particulate material of the Irtysh river, the main
861 tributary of the Ob river, Siberia. Appl. Geochem. **19**, 593-610.
862
863 Haese R. R., Schramm J., van der Loeff M. M. R. and Schulz H. D. (2000) A
864 comparative study of iron and manganese diagenesis in continental slope and deep
865 sea basin sediments off Uruguay (SW Atlantic). Int. J. Earth Sci. **88**, 619-629.
866
867 Hölemann J. A., Schirmacher M. and Prange A. (1995) Transport and distribution of
868 trace elements in the Laptev Sea: first results od the Transdrift expedotions. Rep.
869 Polar Mar. Res. **176,** 297-302.
870
871 Hölemann J. A., Schirmacher M., Kassens H. and Prange A. (1999) Geochemistry of
872 surficial and ice-rafted sediments from the Laptev Sea (Siberia). Estuar. Coast. Shelf
873 Sci. **49**, 45-59.
874
875 Hölemann J. A., Schirmacher M. and Prange A. (2005) Seasonal variability of trace
876 metals in the Lena River and the southeastern Laptev Sea: Impact of the spring
877 freshet. Global Planet. Change **48**, 112-125.
878
879 Homoky W. B., Severmann S., McManus J., Berelson W. M., Riedel T. E., Statham
880 P. J. and Mills R. A. (2012) Dissolved oxygen and suspended particles regulate the

benthic flux of iron from continental margins. Mar. Chem. **134**, 59-70.

Hulth S. et al. (1996) (Tables 1, 3) Pore water chemistry of Arctic surface sediments. doi:10.1594/PANGAEA.78615,
In Supplement to: Hulth S., Hall P., Blackburn T. H. and Landén A. (1996) Arctic sediments (Svalbard): pore water and solid phase distributions of C, N, P and Si. *Polar Biol*. **16**, 447-462.

Hulth S., Aller R. C. and Gilbert F. (1999) Coupled anoxic nitrification/manganese reduction in marine sediments. Geochim. Cosmochim. Acta **63**, 49-66.

Jakobsson M., Andreassen K., Bjarnadottir L. R., Dove D., Dowdeswell J. A., England J. H., Funder S., Hogan K., Ingólfsson Ó., Jennings A., Larsen N. K., Kirchner N., Landvik J. Y., Mayer L., Mikkelsen N., Möller P., Niessen F., Nilsson J., O'Regan M., Polyak L., Norgaard-Pedersen N. and Stein R. (2014) Arctic Ocean glacial history. Quaternary Sci. Rev. **92**, 40-67.

Jakobsson M., Backman J., Rudels B., Nycander J., Frank M., Mayer L., Jokat W., Sangiorgi F., O'Regan M., Brinkhuis H., King J. and Moran K. (2007) The early Miocene onset of a ventilated circulation regime in the Arctic Ocean. Nature **447**, 986-990.

Jakobsson M., Grantz A., Kristoffersen Y. and Macnab R. (2003) Physiographic provinces of the arctic ocean seafloor. Geol. Soc. Am. Bull. **115**, 1443-1455.

906 Jakobsson M., Lovlie R., Al-Hanbali H., Arnold E., Backman J. and Morth M. (2000)
907 Manganese and color cycles in Arctic Ocean sediments constrain Pleistocene
908 chronology. Geology **28**, 23-26.
909
910 Jakobsson M., Lovlie R., Arnold E. M., Backman J., Polyak L., Knutsen J. O. and
911 Musatov E. (2001) Pleistocene stratigraphy and paleoenvironmental variation from
912 Lomonosov Ridge sediments, central Arctic Ocean. Global Planet. Change **31**, 1-22.
913
914 Johnson C. M., Beard B. L. and Roden E. E. (2008) The iron isotope fingerprints of
915 redox and biogeochemical cycling in the modern and ancient Earth. Ann. Rev. Earth
916 Pl. Sci. **36**, 457-493.
917
918 Jokat W. (2009) The Expedition ARK-XXIII/3 of RV Polarstern in 2008. Rep. Polar
919 Mar. Res. **597**.
920
921 Kiczka M., Wiederhold J. G., Frommer J., Voegelin A., Kraemer S. M., Bourdon B.
922 and Kretzschmar R. (2011) Iron speciation and isotope fractionation during silicate
923 weathering and soil formation in an alpine glacier forefield chronosequence.
924 Geochim. Cosmochim. Acta **75**, 5559-5573.
925
926 Klunder M. B., Bauch D., Laan P., de Baar H. J. W., van Heuven S. and Obe, S.
927 (2012) Dissolved iron in the Arctic shelf seas and surface waters of the central Arctic
928 Ocean: Impact of Arctic river water and ice-melt. J. Geophys. Res.-Oceans **117**.
929
930 Knauer G. A., Martin J. H. and Gordon R. M. (1982) Cobalt in north-east Pacific
931 Waters. Nature **297**, 49-51.

Kuma K., Takata H., Kitayama S. and Omata A. (2013) Water Column Iron Dynamics in the North Pacific Ocean, Bering Sea and Western Arctic Ocean. Bunseki Kagaku **62**, 1057-1069.

Lambeck K., Esat T. M. and Potter E. K. (2002) Links between climate and sea levels for the past three million years. Nature **419**, 199-206.

Lettmann K. A., Riedinger N., Ramlau R., Knab N., Bottcher M. E., Khalili A., Wolff J. O. and Jorgensen B. B. (2012) Estimation of biogeochemical rates from concentration profiles: A novel inverse method. Estuar. Coastal Shelf Sci. **100**, 26-37.

Li Y. H., Bischoff J. and Mathieu G. (1969) The Migration of Manganese in the Arctic Basin Sediment. Earth Planet. Sci. Lett. **7**, 265-270.

Li Y. H. and Gregory S. (1974) Diffusion of Ions in Sea-Water and in Deep-Sea Sediments. Geochim. Cosmochim. Acta **38**, 703-714.

Lovley D. R. and Phillips E. J. P. (1988) Novel Mode of Microbial Energy Metabolism: Organic Carbon Oxidation Coupled to Dissimilatory Reduction of Iron or Manganese. Appl. Environ. Microb. **54**, 1472-1480.

Löwemark L., März C., O'Regan M. and Gyllencreutz R. (2014) Arctic Ocean Mn-stratigraphy: genesis, synthesis and inter-basin correlation. Quaternary Sci. Rev. **92**, 97-111.

Löwemark L., O'Regan M., Hanebuth T. J. J. and Jakobsson M. (2012) Late Quaternary spatial and temporal variability in Arctic deep-sea bioturbation and its relation to Mn cycles. Palaeogeogr. Palaeocl. Palaeoeco. **365**, 192-208.

Macdonald R. W. and Gobeil C. (2012) Manganese Sources and Sinks in the Arctic Ocean with Reference to Periodic Enrichments in Basin Sediments. Aquat. Geochem. **18**, 565-591.

März C., Meinhardt A.-K., Schnetger B. and Brumsack H.-J. (2015) Silica diagenesis and benthic fluxes in the Arctic Ocean. Mar. Chem. **171**, 1-9.

März C., Poulton S. W., Brumsack H.-J. and Wagner T. (2012) Climate-controlled variability of iron deposition in the Central Arctic Ocean (southern Mendeleev Ridge) over the last 130,000 years. Chem. Geol. **330**, 116-126.

März C., Schnetger B. and Brumsack H.-J. (2010) Paleoenvironmental implications of Cenozoic sediments from the central Arctic Ocean (IODP Expedition 302) using inorganic geochemistry. Paleoceanography **25**, PA3206.

März C., Stratmann A., Matthiessen J., Meinhardt A.-K., Eckert S., Schnetger B., Vogt C., Stein R. and Brumsack H.-J. (2011) Manganese-rich brown layers in Arctic Ocean sediments: Composition, formation mechanisms, and diagenetic overprint. Geochim. Cosmochim. Acta **75**, 7668-7687.

Mansfeldt T., Schuth S., Hausler W., Wagner F. E., Kaufhold S. and Overesch M. (2012) Iron oxide mineralogy and stable iron isotope composition in a Gleysol with petrogleyic properties. J. Soil. Sediment. **12**, 97-114.

Meinhardt A.-K., März C., Stein R. and Brumsack H.-J. (2014) Regional variations in sediment geochemistry on a transect across the Mendeleev Ridge (Arctic Ocean). Chem. Geol. **369**, 1-11.

Martin J. M., Guan D. M., Elbazpoulichet F., Thomas A. J. and Gordeev V. V. (1993) Preliminary Assessment of the Distributions of Some Trace-Elements (as, Cd, Cu, Fe, Ni, Pb and Zn) in a Pristine Aquatic Environment - the Lena River Estuary (Russia). Mar. Chem. **43**, 185-199.

Matthiessen J. (2011) Documentation of sediment core PS78/248-6. doi:10.1594/PANGAEA.771320

Middag R., de Baar H. J. W., Laan P. and Klunder M. B. (2011) Fluvial and hydrothermal input of manganese into the Arctic Ocean. Geochim. Cosmochim. Acta **75**, 2393-2408.

Morford J. L. and Emerson S. (1999) The geochemistry of redox sensitive trace metals in sediments. Geochim. Cosmochim. Acta **63**, 1735-1750.

Murray J. W. (1975) The interaction of metal ions at the manganese dioxide-solution interface. Geochim. Cosmochim. Acta **39**, 505-519.

1008 Murray J. W. and Dillard J. G. (1979) The oxidation of cobalt(II) adsorbed on
1009 manganese dioxide. Geochim. Cosmochim. Acta **43**, 781-787.
1010
1011 Nakayama Y., Fujita S., Kuma K. and Shimada K. (2011) Iron and humic-type
1012 fluorescent dissolved organic matter in the Chukchi Sea and Canada Basin of the
1013 western Arctic Ocean. J. Geophys. Res.-Oceans **116**.
1014
1015 Nolting R. F., vanDalen M. and Helder W. (1996) Distribution of trace and major
1016 elements in sediment and pore waters of the Lena Delta and Laptev Sea. Mar.
1017 Chem. **53**, 285-299.
1018
1019 Oeser M., Weyer S., Horn I. and Schuth S. (2014) High-Precision Fe and Mg Isotope
1020 Ratios of Silicate Reference Glasses Determined In Situ by Femtosecond LA-MC-
1021 ICP-MS and by Solution Nebulisation MC-ICP-MS. Geostand. Geoanal. Res. **38**,
1022 311-328.
1023
1024 Poitrasson F. and Freydier R. (2005) Heavy iron isotope composition of granites
1025 determined by high resolution MC-ICP-MS. Chem. Geol. **222**, 132-147.
1026
1027 Pokrovsky O. S., Viers J., Shirokova L. S., Shevchenko V. P., Filipov A. S. and Dupre
1028 B. (2010) Dissolved, suspended, and colloidal fluxes of organic carbon, major and
1029 trace elements in the Severnaya Dvina River and its tributary. Chem. Geol. **273**, 136-
1030 149.
1031
1032 Rachold V., Alabyan A., Hubberten H. W., Korotaev V. N. and Zaitsev A. A. (1996)
1033 Sediment transport to the Laptev Sea - Hydrology and geochemistry of the Lena

River. Polar Res. **15**, 183-196.

Reeder S. W., Hitchon B. and Levinson A. A. (1972) Hydrogeochemistry of the surface waters of the Mackenzie River drainage basin, Canada-1. Factors controlling inorganic composition. Geochim. Cosmochim. Acta **36**, 825-865.

Schauer U. (2012) The expedition of the research vessel "Polarstern" to the Arctic in 2011 (ARK-XXVI/3 - TransArc). Rep. Polar Mar. Res. **649**.

Schnetger B. and Lehners C. (2014) Determination of nitrate plus nitrite in small volume marine water samples using vanadium(III)chloride as a reduction agent. Mar. Chem. **160**, 91-98.

Scholz F., Severmann S., McManus J. and Hensen C. (2014) Beyond the Black Sea paradigm: The sedimentary fingerprint of an open-marine iron shuttle. Geochim. Cosmochim. Acta **127**, 368-380.

Schuth S., Hurraß J., Münker C. and Mansfeldt T. (2015) Redox-dependent fractionation of iron isotopes in suspensions of a groundwater-influenced soil. Chem. Geol. **392**, 74-86.

Schulz H. D. (2006) Quantification of Early Diagenesis: Dissolved Constituents in Marine Pore Water, in: Schulz H. D. and Zabel M. (Eds.) Marine Geochemistry, Springer Verlag Berlin Heidelberg.

Seeberg-Elverfeldt J., Schlüter M., Feseker T. and Kölling M. (2005) Rhizon sampling

of porewaters near the sediment-water interface of aquatic systems. Limnol. Oceanogr.-Meth. **3**, 361-371.

Severmann S., Johnson C. M., Beard B. L. and McManus J. (2006) The effect of early diagenesis on the Fe isotope compositions of porewaters and authigenic minerals in continental margin sediments. Geochim. Cosmochim. Acta **70**, 2006-2022.

Severmann S., Lyons T. W., Anbar A., McManus J. and Gordon G. (2008) Modern iron isotope perspective on the benthic iron shuttle and the redox evolution of ancient oceans. Geology **36**, 487-490.

Shaw T. J., Gieskes J. M. and Jahnke R. A. (1990) Early diagenesis in differing depositional evironments: The response of transition metals in pore water. Geochim. Cosmochim. Acta **54**, 1233-1246.

Shimmield G. B. and Price N. B. (1986) The Behavior of Molybdenum and Manganese during Early Sediment Diagenesis - Offshore Baja-California, Mexico. Mar. Chem. **19**, 261-280.

Spielhagen R. F., Baumann K. H., Erlenkeuser H., Nowaczyk N. R., Norgaard-Pedersen N., Vogt C. and Weiel D. (2004) Arctic Ocean deep-sea record of northern Eurasian ice sheet history. Quaternary Sci. Rev. **23**, 1455-1483.

Stein R. (2008) Arctic Ocean Sediments: Processes, Proxies, and Paleoenvironment. Developments in Marine Geology 2, Elsevier.

1086

1087 Stein R., Usbeck R. and Polozek K. (2004) Physical properties of sediment core

1088 PS51/058-3. doi:10.1594/PANGAEA.205436

1089

1090 Strekopytov S. V. (2003) Geochemistry of diagenesis of sediments in the Barents

1091 Sea: Forms of iron and sulfur. Lithol. Miner. Resour. **38**, 1-11.

1092

1093 Sundby B., Lecroart P., Anschutz P., Katsev S. and Mucci A. (2015) When deep

1094 diagenesis in Arctic Ocean sediments compromises manganese-based

1095 geochronology. Mar. Geol. **366**, 62-68.

1096

1097 Thuroczy C. E., Gerringa L. J. A., Klunder M., Laan P., Le Guitton M. and de Baar H.

1098 J. W. (2011) Distinct trends in the speciation of iron between the shallow shelf seas

1099 and the deep basins of the Arctic Ocean. J. Geophys. Res.-Oceans **116**.

1100

1101 Tovar-Sánchez A., Duarte C. M., Alonso J. C., Lacorte S., Tauler R. and Galbán-

1102 Malagón C. (2010) Impacts of metals and nutrients released from melting multiyear

1103 Arctic sea ice. J. Geophys. Res.-Oceans **115**.

1104

1105 Tribovillard N., Algeo T. J., Lyons T., Riboulleau A., 2006. Trace metals as

1106 paleoredox and paleoproductivity proxies: An update. Chem. Geol. **232** (1-2), 12-32.

1107

1108 Turekian K. K. and Wedepohl K. H. (1961) Distribution of the Elements in Some

1109 Major Units of the Earth's Crust. Geol. Soc. Am. Bull. **72**, 175-192.

1110

1111 Turner R. R. and Harriss R. C. (1970) The distribution of non-detrital iron and

manganese in two cores from the Kara Sea. Deep-Sea Res. **17**, 633-636.

Wagemann R., Brunskill G. J. and Graham B. W. (1977) Composition and Reactivity of Some River Sediments from the Mackenzie Valley, N.W.T., Canada. Environ. Geol. **1**, 349-358.

Wedepohl K. H. (1971) Environmental influences on the chemical composition of shales and clays. In: Ahrens L. H., Press F., Runcorn S. K. and Urey H. C. (eds), Physics and Chemistry of the Earth, vol. 8. Pergamon Press, Oxford, p. 307-333.

Wedepohl K. H. (1991) The Composition of the Upper Earth's Crust and the Natural Cycles of Selected Metals. Metals in Natural Raw Materials. Natural Resources. In: Merian E. (ed), Metals and their Compounds in the Natural Environment, VCH-Verlag, Weinheim, p. 1-17.

Weyer S. and Schwieters J. (2003) High precision Fe isotope measurements with high mass resolution MC-ICPMS. Int. J. Mass Spectrom. **226**, 355-368.

Zhuang G. S., Yi Z. and Wallace G. T. (1995) Iron(II) in rainwater, snow, and surface seawater from a coastal environment. Mar. Chem. **50**, 41-50.

Table captions

Table 1: Core locations, δ^{56}Fe values, Fe/Al, and ratios of lithogenic and non-lithogenic Fe. Star marks core without δ^{56}Fe measurement.

1138 Table 2: Parameters and references for the Fe budget. [a]Wagemann et al., 1977;
1139 Gaillardet et al., 1999. [b]Reeder et al. 1972. [c]Nolting et al., 1996; Rachold et al., 1996;
1140 Gordeev et al., 2004; Hölemann et al., 2005. [d]Martin et al., 1993; Hölemann et al.,
1141 1995; 1999; 2005; Pokrovsky et al., 2010. [e]Average b and d. [f]3% of the global
1142 estimate from Duce and Tindale, 1991, and Zhuang et al., 1995. [g]Aguilar-Islas et al.,
1143 2007; Kuma et al., 2013. [h]Klunder et al., 2012. [i]Turekian and Wedepohl, 1961. [j]See
1144 chapter 3.7.1. [k]Strekopytov 2003. [l]Data from cores 206-3, 220-7, 237-3, and 248-6.
1145
1146 Table 3: Sedimentary Mn_{xs} and Fe_{xs} calculations for four different sediment cores.
1147
1148 Table 4: Boundary parameters used for the calculation of diffusive fluxes of cores
1149 248-6, 206-3, and 220-7. D_{sw} for Mn and Co from Boudreau (1997). D_{sw} for Mo
1150 estimated from Li and Gregory (1974). See chapter 4.3 and Appendix for details.
1151
1152 Figure captions
1153
1154 Figure 1: Map of the core locations.
1155
1156 Figure 2: Stratigraphic correlation of core 248-6 to three sediment cores (LRG09-
1157 GC03; 96/12-1PC; ACEX core) from the central Lomonosov Ridge (from Löwemark
1158 et al., 2014). Horizontal gray bars: gray sediment layers in core 248-6. Gray
1159 patterned intervals mark coarse-grained diamicts. Stippled vertical gray bar: zone of
1160 low Mn abundance in the diamicts.
1161
1162 Figure 3: Sedimentary Mn/Al, Fe/Al, Co/Al, Mo/Al, and Ni/Al values (black) and pore
1163 water Mn^{2+}, Co^{2+}, Mo^{6+} (all red), NO_3^- (blue), SO_4^{2-} (green) and NH_4^+ (orange)

concentrations in core 248-6. Dashed black line represents average shale (Wedepohl 1971, 1991), dashed red line represents mean Arctic seawater Mo value (Tovar-Sánchez et al., 2010), gray bars represent gray sediment layers, brown bars represent dark brown sediment layers.

Figure 4: X-ray radiographs, Mn_{xs} contents, and core photos of core 248-6 (x-ray radiographs and photos: Matthiessen, 2011). Thin white bands in the x-ray radiographs correspond to higher Mn_{xs} contents and dark brown sediment color.

Figure 5: Sedimentary Mn/Al, Fe/Al, Co/Al, Mo/Al, and Ni/Al values (black) and pore water Mn^{2+}, Co^{2+}, Mo^{6+} (all red), NO_3^- (blue), SO_4^{2-} (green) and NH_4^+ (orange) concentrations in core 206-3. For additional information see Fig. 3.

Figure 6: Sedimentary Mn/Al, Fe/Al, Co/Al, Mo/Al, and Ni/Al values (black) and pore water Mn^{2+}, Co^{2+}, Mo^{6+} (all red), NO_3^- (blue), SO_4^{2-} (green) and NH_4^+ (orange) concentrations in core 220-7. For additional information see Fig. 3.

Figure 7: Sedimentary Mn/Al, Fe/Al, Co/Al, Mo/Al, and Ni/Al values (black) and pore water Mn^{2+}, Co^{2+}, Mo^{6+} (all red), NO_3^- (blue), SO_4^{2-} (green) and NH_4^+ (orange) concentrations in core 237-3. For additional information see Fig. 3.

Figure 8: Fe/Al (black) and $\delta^{56}Fe$ values (blue) of sediment cores 206, 237, 248, 410 (gravity corer and multicorer), 275, 277, 280, and 285 (multicorer). See also Table 1. Dashed black line represents average shale (Wedepohl 1971, 1991), blue line represents $\delta^{56}Fe = 0$, gray bars represent gray sediment layers, brown bars represent dark brown sediment layers.

Figure 9: Fe/Al relative to δ^{56}Fe values. Residual Fe in the gray layers is isotopically heavier, indicating the lithogenic background. Fe-rich samples and surface samples are isotopically lighter, indicating a mobile Fe fraction.

Figure 10: Co_{xs} versus Mo_{xs} relationship of different dark brown sediment layers. a) core 248-6, b) core 206-3, c) core 220-7, d) 237-3. Layers with diagenetic addition of Mn from the pore water have lower Co_{xs}/Mo_{xs}. Layers that were subjected to Mn reduction have higher ratios.

Figure 11: Net Mn^{2+} rate of core 248-6 from the REC model (Lettmann et al., 2012). Positive values indicate Mn^{2+} production and negative values indicate Mn^{2+} consumption.

Appendix

Example for the calculation of the Mn accumulation rate, pore water fluxes and pore water flux derived Mn_{xs} in core 248-6.

Table1

Sample	Latitude	Longitude	Water depth (m)	Depth in core (cm)	^{56}Fe (‰)	±2sd	Fe/Al	Fe_{Lith}/Fe_{NL}
PS78/206-2 MUC	86° 26,43' N	60° 5,75' E	1770	0-1	0.109	0.031	0.51	31.9
PS78/206-3 GC	86° 26,55' N	60° 9,27' E	1791	41-42	0.082	0.026	0.46	2.1
PS78/206-3 GC				49-50	-0.220	0.019	0.85	0.6
PS78/206-3 GC				141-142	0.167	0.029	0.32	46.5
PS78/206-3 GC				251-252	0.160	0.034	0.66	0.9
PS78/237-1 MUC	83° 44,65' N	154° 24,88' W	2378	1-2	0.052	0.034	0.57	4.2
PS78/237-3 GC	83° 44,85' N	154° 25,64' W	2369	15-16	0.119	0.013	0.52	3.8
PS78/237-3 GC				25-26	0.059	0.019	0.60	3.7
PS78/237-3 GC				37-38	0.104	0.031	0.58	4.4
PS78/237-3 GC				46-47	0.085	0.01	0.58	4.6
PS78/248-4 MUC	84° 40,75' N	149° 59,41' E	1611	0-1	0.030	0.009	0.64	6.0
PS78/248-6 GC	84° 40,37' N	149° 47,79' E	1620	44-45	0.034	0.047	0.61	1.5
PS78/248-6 GC				120-121	0.235	0.039	0.38	26.9
PS78/248-6 GC				463-464	-0.072	0.033	0.86	0.8
PS78/248-6 GC				481-482	0.274	0.011	0.37	124.9
PS78/275-1 MUC	80° 49,13' N	120° 58,26' E	3527	0-1	-0.006	0.022	0.62	8.4
PS78/277-2 MUC	80° 12,54' N	122° 12,20' E	3359	0-1	0.035	0.034	0.63	8.8
PS78/280-6 MUC	79° 8,97' N	124° 2,11' E	3077	0-1	0.069	0.006	0.58	5.4
PS78/285-6 MUC	78° 29,97' N	125° 42,94' E	2805	0-1	-0.057	0.074	0.67	6.4
PS72/410-2 MUC	80° 31,04' N	175° 44,07' W	1828	0-1	0.083	0.03	0.59	4.5
PS72/410-2 MUC				11-12	0.074	0.075	0.57	5.6
PS72/410-3 GC	80° 31,39' N	175° 43,18' W	1854	18-19	0.014	0.023	0.60	4.1
PS72/410-3 GC				34-35	0.103	0.026	0.50	68.9
PS72/410-3 GC				38-39	0.059	0.032	0.59	4.6
PS72/410-3 GC				55-56	0.052	0.031	0.53	only Lith
PS72/410-3 GC				64-65	0.032	0.039	0.60	9.8
PS78/220-7 GC*	89° 14,86' N	115° 11,34' W	1668					

Table2

		Dissolved µg/l	Particulate µg/g	Dissolved kt/a	Particulate kt/a	Total kt/a
Inputs						
Mackenzie	total		36,075[a]		4,473	
	lithogenic		28,860		3,579	3,579
	non-lithogenic	20[b]	7,215	7	895	901
Siberian rivers	total		48,864[c]		5,033	
	lithogenic		39,092		4,026	4,026
	non-lithogenic	169[d]	9,773	502	1,007	1,508
Groundwater	non-lithogenic	94[e]		28		28
Atmospheric	total				870[f]	
	lithogenic				696	2,560
	non-lithogenic	0.2[f]		1	174	175
Pacific inflow	non-lithogenic	0.14[g]		4		4
Atlantic inflow	non-lithogenic	0.039[h]		4		4
Coastal erosion	lithogenic		37,760[i]		16,237	16,237
	non-lithogenic		9,440[i]		4,059	4,059
Hydrothermal	non-lithogenic					100[j]
Total	lithogenic					24,538
	non-lithogenic					6,779
	total					**31,317**
Outputs						
Atlantic outflow	non-lithogenic	0.039[h]		-4		-4
CAA outflow	non-lithogenic	0.039[h]		-1		-1
Ice export	lithogenic		37,760[i]		-325	-325
	non-lithogenic		9,440[i]		-81	-81
Sediment export	lithogenic		37,760[i]		-1,850	-1,850
	non-lithogenic		9,440[i]		-463	-463
Shelf sediments	lithogenic		47,761[k]		-22,113	-22,113
	non-lithogenic		11,427[k]		-5,291	-5,291
Basin sediments	lithogenic		29,000[l]		-4,118	-4,118
	non-lithogenic		11,848[l]		-1,682	-1,682
Total	lithogenic					-28,406
	non-lithogenic					-7,522
	total					**-35,929**

Table3

	248-6	206-3	220-7	ACEX
mean Mn_{xs} ($g*kg^{-1}$)	4135	1000	820	1940
sedimentation rate ($cm*a^{-1}$)	0.0036	0.0018	0.0010	0.0024
Mn accumulation rate ($g*cm^{-2}*a^{-1}$)	1.69E-05	2.11E-06	9.08E-07	5.40E-06
Mn from external sources (rel-%)	48	>100	>100	>100
mean Fe_{xs} ($mg*kg^{-1}$)	18757	12520	33010	23210
Fe accumulation rate ($g*cm^{-2}*a^{-1}$)	7.67E-05	2.64E-05	3.66E-05	6.46E-05
Fe from external sources (rel-%)	>100	>100	>100	>100

Table4

Core	element	Φ	θ^2	$D_{sw}^{0°C}$ (m^2*s^{-1})	D_{sed} (m^2*s^{-1})	gradient ($mol*m^{-4}$)	J_{sed} ($mol*m^{-2}*a^{-1}$)	representative time for flux (ka)	total $element_{xs}$ ($g*kg^{-1}$)	flux-derived $element_{xs}$ ($g*kg^{-1}$)	flux-derived $element_{xs}$ (rel-%)
248-6	Mn	0.6	2.02	$3.0*10^{-10}$	$1.5*10^{-10}$	$2.1*10^{-1}$	$0.6*10^{-3}$	120	9.1	13.5	149
								12	9.1	1.3	15
	Co	0.6	2.02	$3.2*10^{-10}$	$1.6*10^{-10}$	$2.6*10^{-4}$	$0.8*10^{-6}$	80	0.021	0.013	61
								12	0.021	0.002	9
	Mo	0.6	2.02	$4.0*10^{-10}$	$2.0*10^{-10}$	$8.7*10^{-4}$	$3.3*10^{-6}$	80	0.029	0.087	303
								12	0.029	0.013	45
206-3	Mn	0.6	2.02	$3.0*10^{-10}$	$1.5*10^{-10}$	$2.2*10^{-2}$	$6.2*10^{-5}$				
220-7	Mn	0.6	2.02	$3.0*10^{-10}$	$1.5*10^{-10}$	$5.6*10^{-2}$	$1.6*10^{-4}$				

Figure1

Click here to download high resolution image

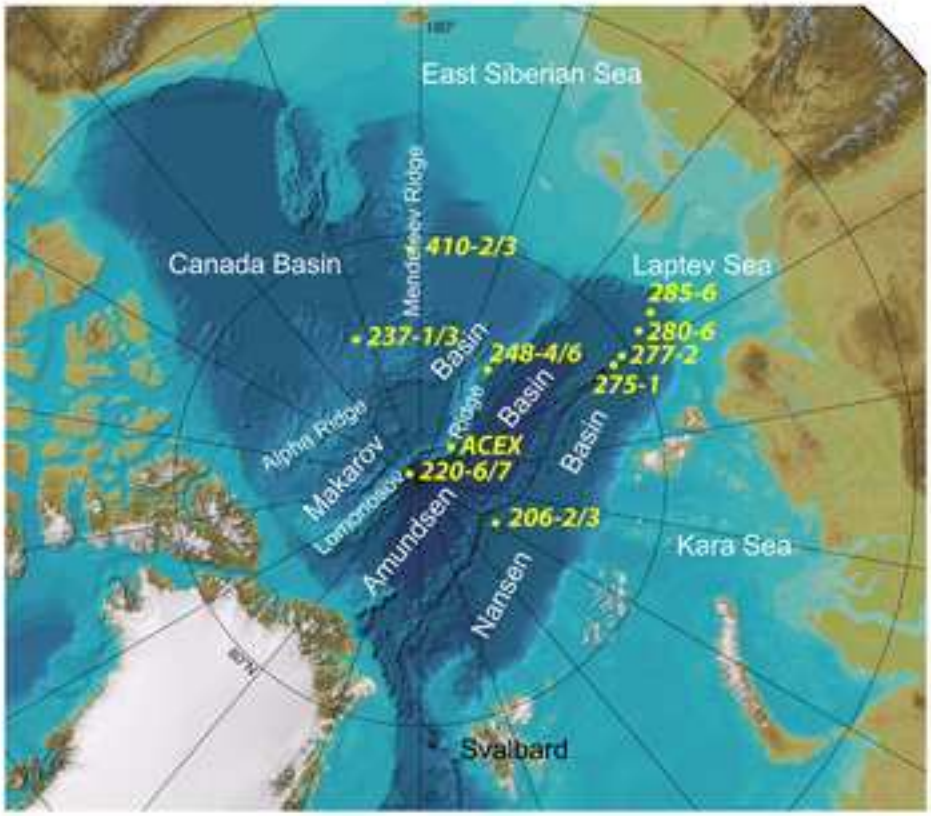

Figure2

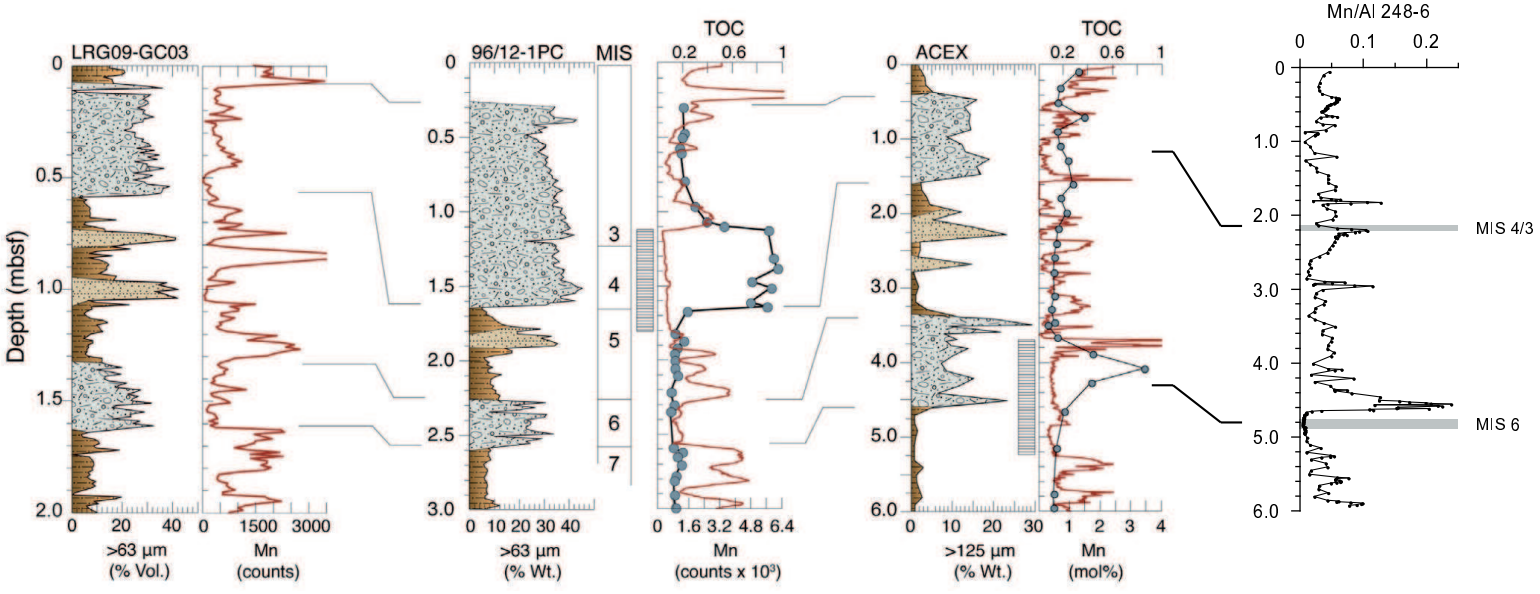
LRG09-GC03
96/12-1PC
MIS
TOC
ACEX
TOC
Mn/Al 248-6
Depth (mbsf)
>63 µm
(% Vol.)
Mn
(counts)
>63 µm
(% Wt.)
Mn
(counts x 10³)
>125 µm
(% Wt.)
Mn
(mol%)
MIS 4/3
MIS 6

Figure3

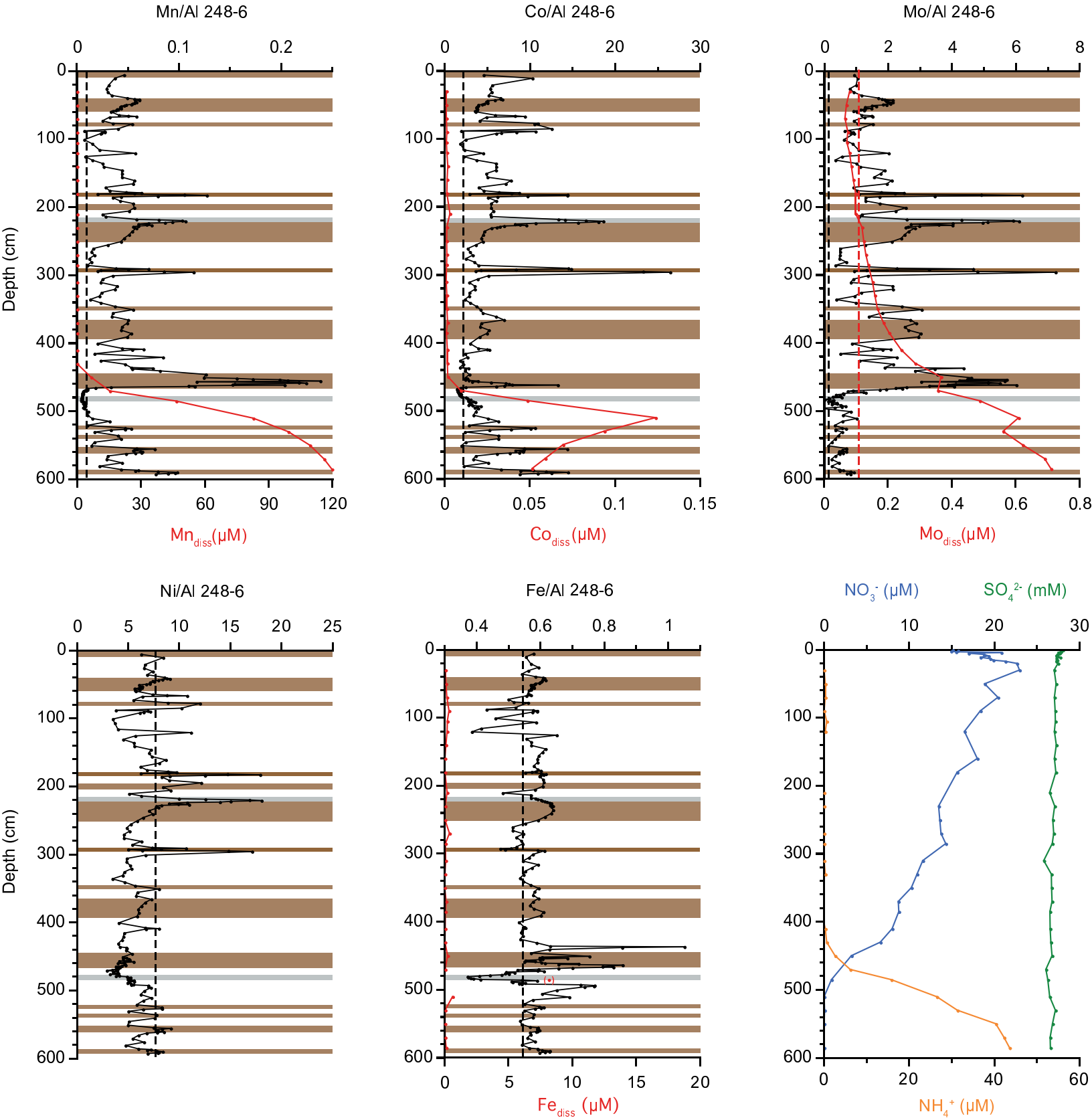
Mn/Al 248-6
Co/Al 248-6
Mo/Al 248-6
Depth (cm)
Mn$_{diss}$(μM)
Co$_{diss}$(μM)
Mo$_{diss}$(μM)
Ni/Al 248-6
Fe/Al 248-6
NO$_3^-$ (μM)
SO$_4^{2-}$ (mM)
Fe$_{diss}$ (μM)
NH$_4^+$ (μM)

Figure4

Click here to download high resolution image

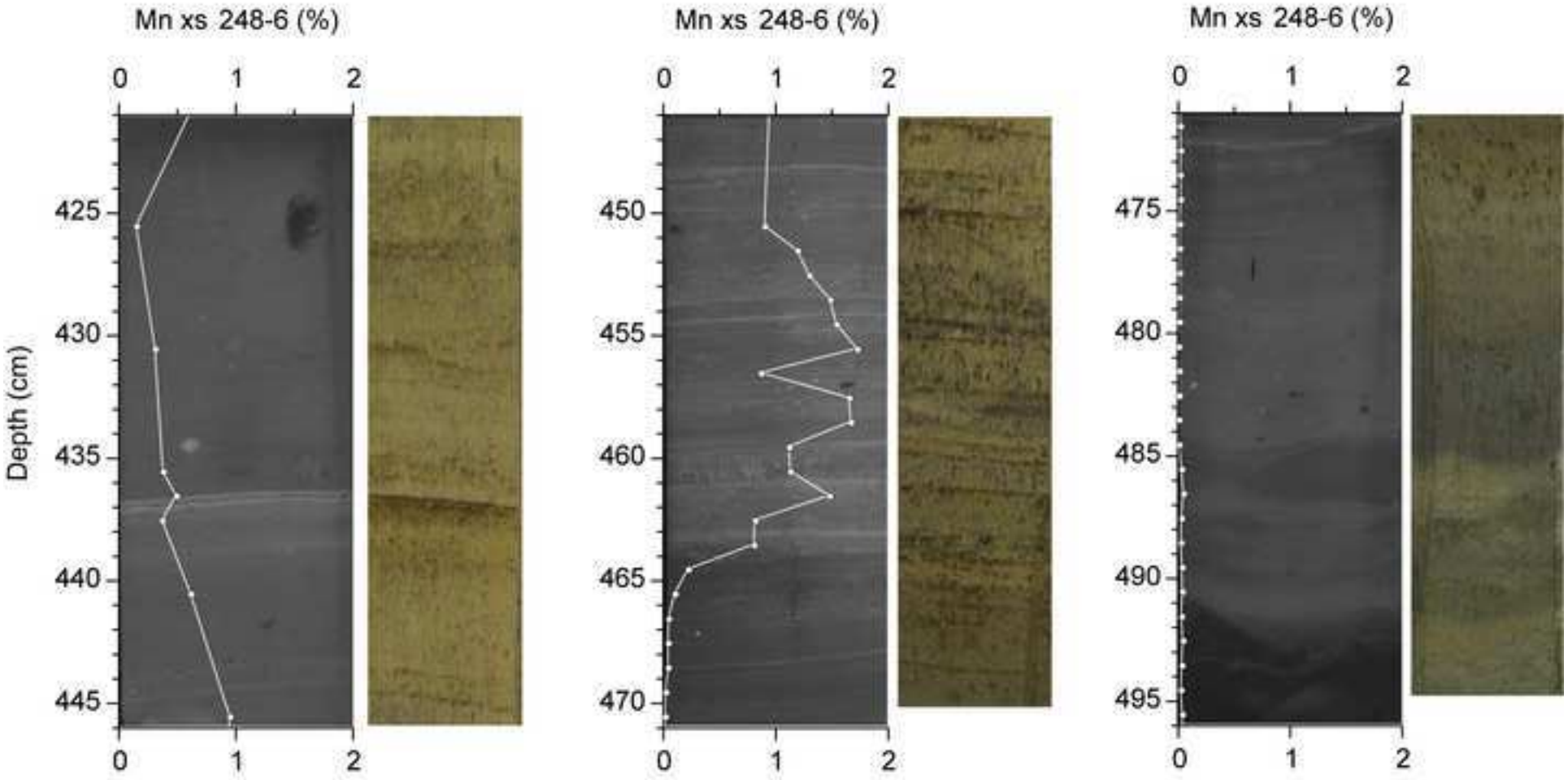

Figure5

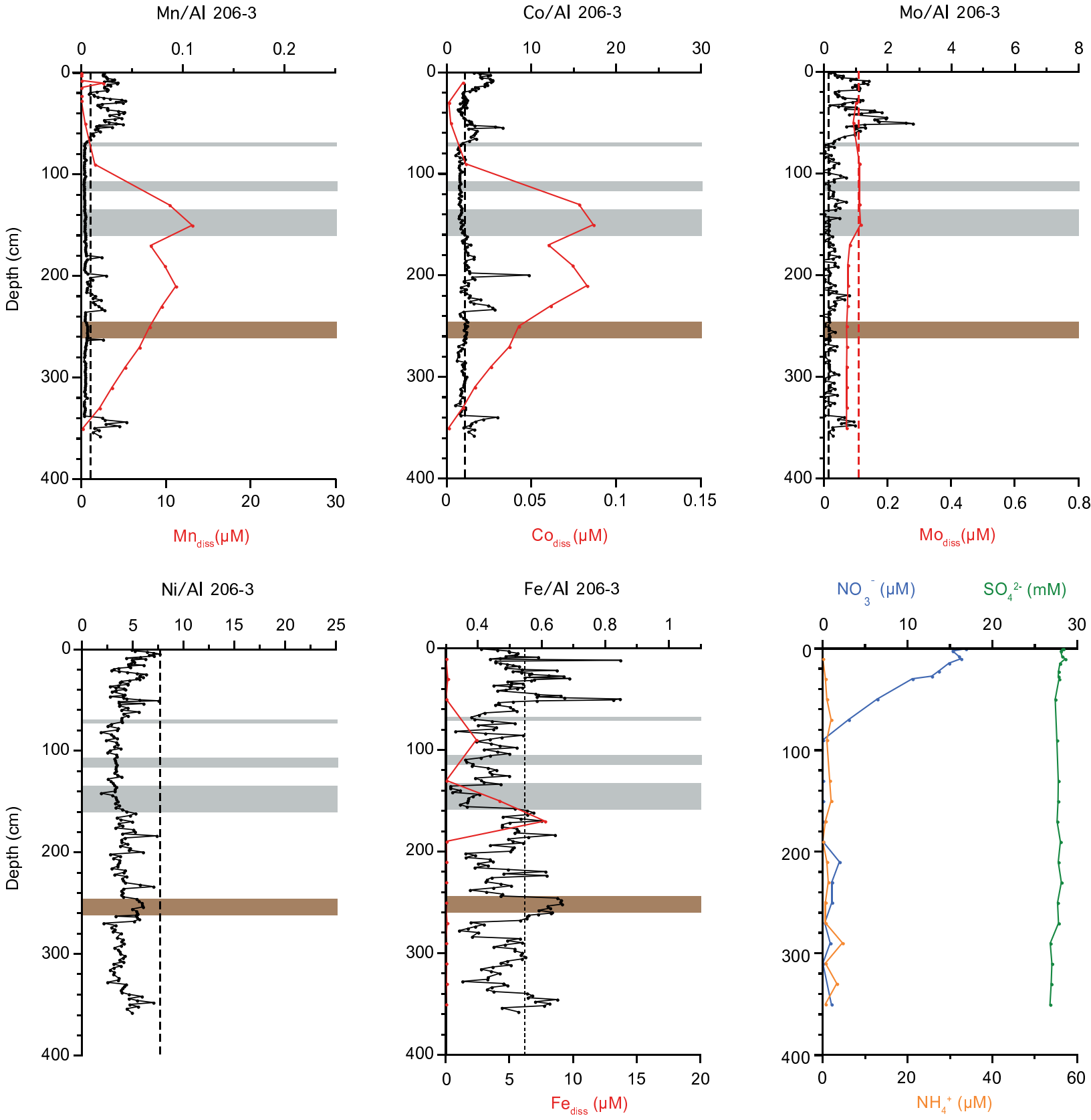
Mn/Al 206-3
Co/Al 206-3
Mo/Al 206-3
Ni/Al 206-3
Fe/Al 206-3
Depth (cm)
Mn$_{diss}$(μM)
Co$_{diss}$(μM)
Mo$_{diss}$(μM)
Fe$_{diss}$ (μM)
NO$_3^-$ (μM)
SO$_4^{2-}$ (mM)
NH$_4^+$ (μM)

Figure6

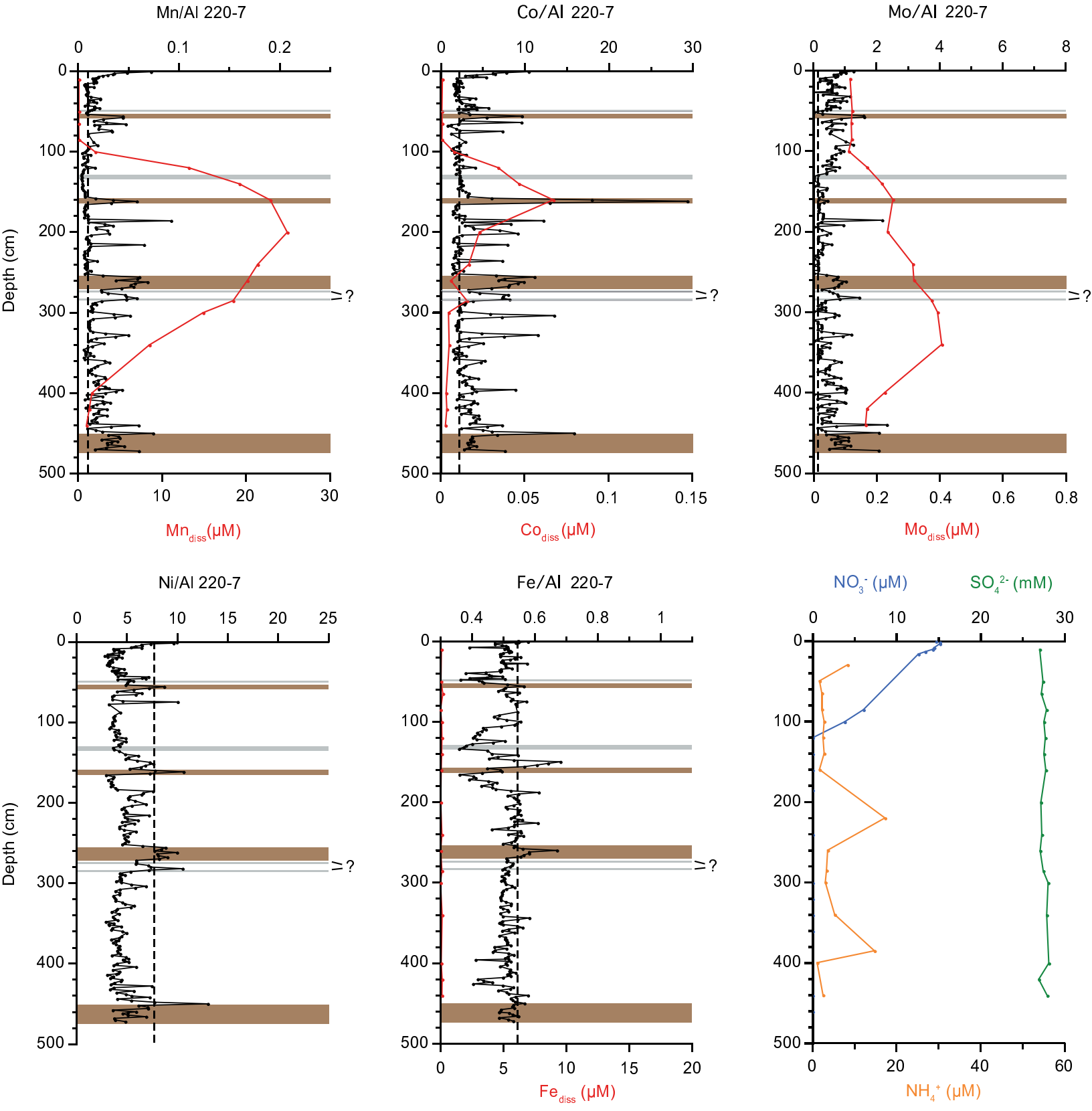
Mn/Al 220-7
Co/Al 220-7
Mo/Al 220-7
Ni/Al 220-7
Fe/Al 220-7
Depth (cm)
Mn$_{diss}$(μM)
Co$_{diss}$ (μM)
Mo$_{diss}$(μM)
Fe$_{diss}$ (μM)
NO$_3^-$ (μM)
SO$_4^{2-}$ (mM)
NH$_4^+$ (μM)
?

Figure7

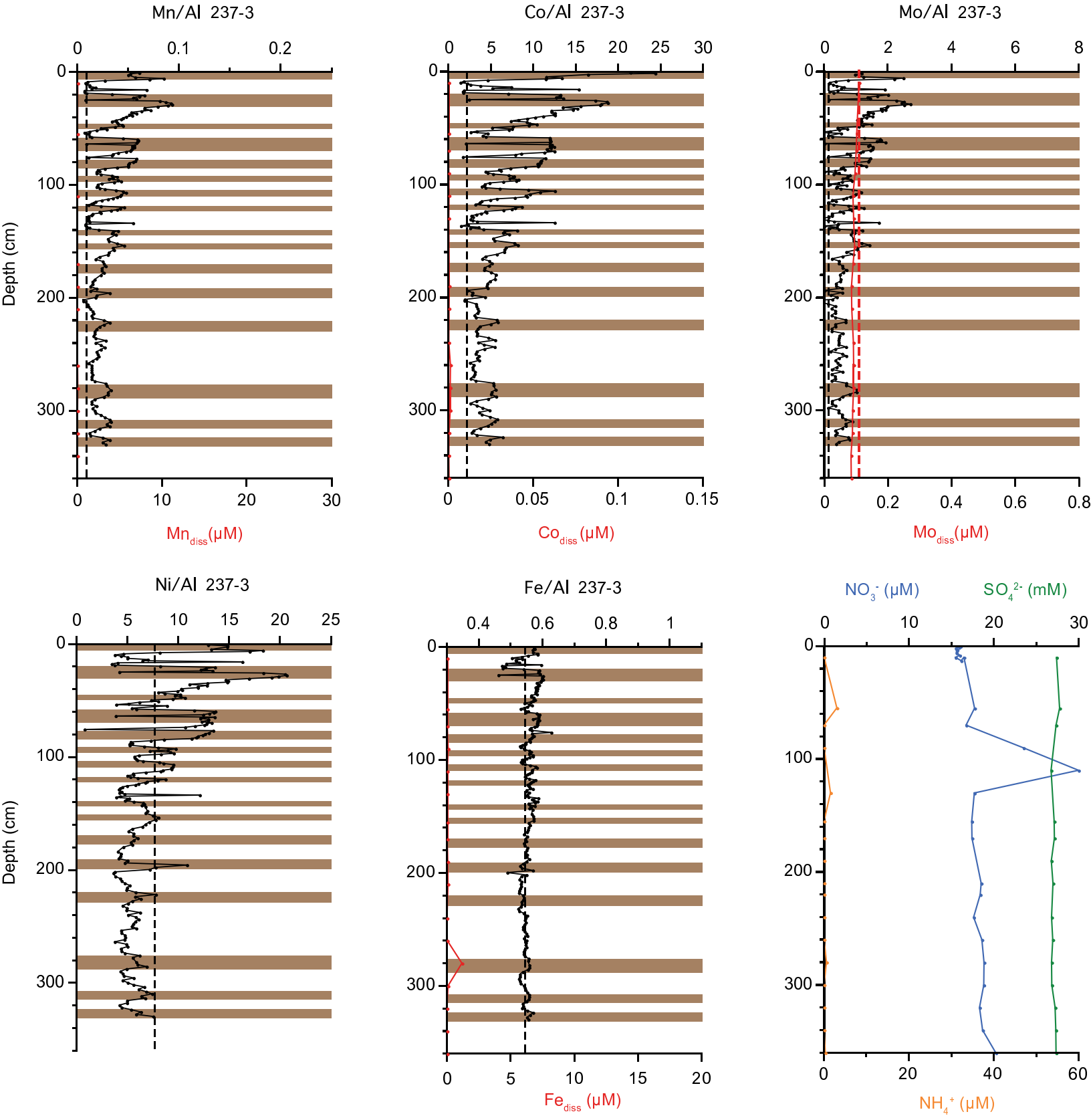
Mn/Al 237-3
Co/Al 237-3
Mo/Al 237-3
Ni/Al 237-3
Fe/Al 237-3
Depth (cm)
Mn$_{diss}$(μM)
Co$_{diss}$ (μM)
Mo$_{diss}$(μM)
Fe$_{diss}$ (μM)
NO$_3^-$ (μM)
SO$_4^{2-}$ (mM)
NH$_4^+$ (μM)

Figure8

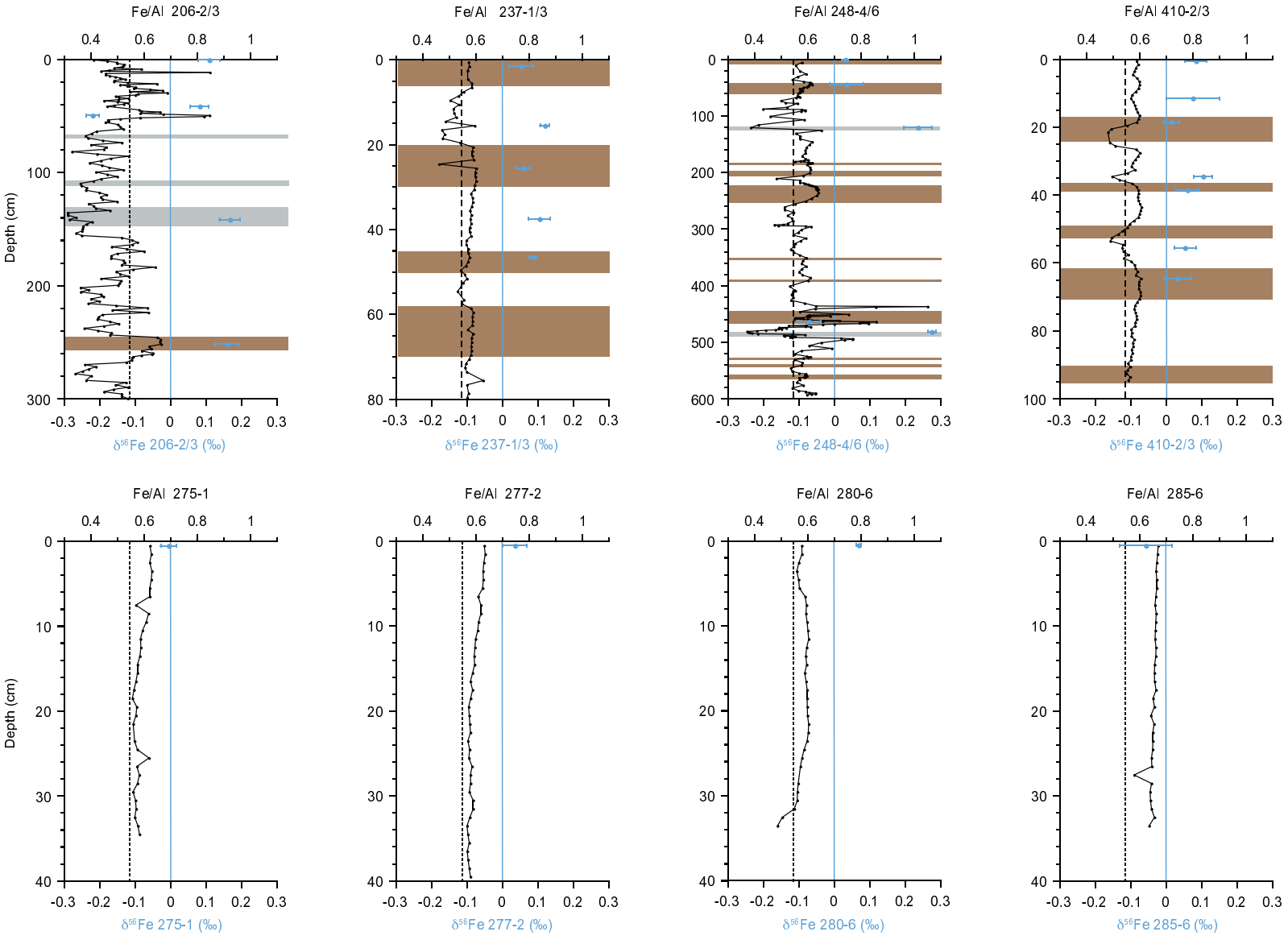
Fe/Al 206-2/3
Fe/Al 237-1/3
Fe/Al 248-4/6
Fe/Al 410-2/3
Fe/Al 275-1
Fe/Al 277-2
Fe/Al 280-6
Fe/Al 285-6
Depth (cm)
δ56Fe 206-2/3 (‰)
δ56Fe 237-1/3 (‰)
δ56Fe 248-4/6 (‰)
δ56Fe 410-2/3 (‰)
δ56Fe 275-1 (‰)
δ56Fe 277-2 (‰)
δ56Fe 280-6 (‰)
δ56Fe 285-6 (‰)

Figure9

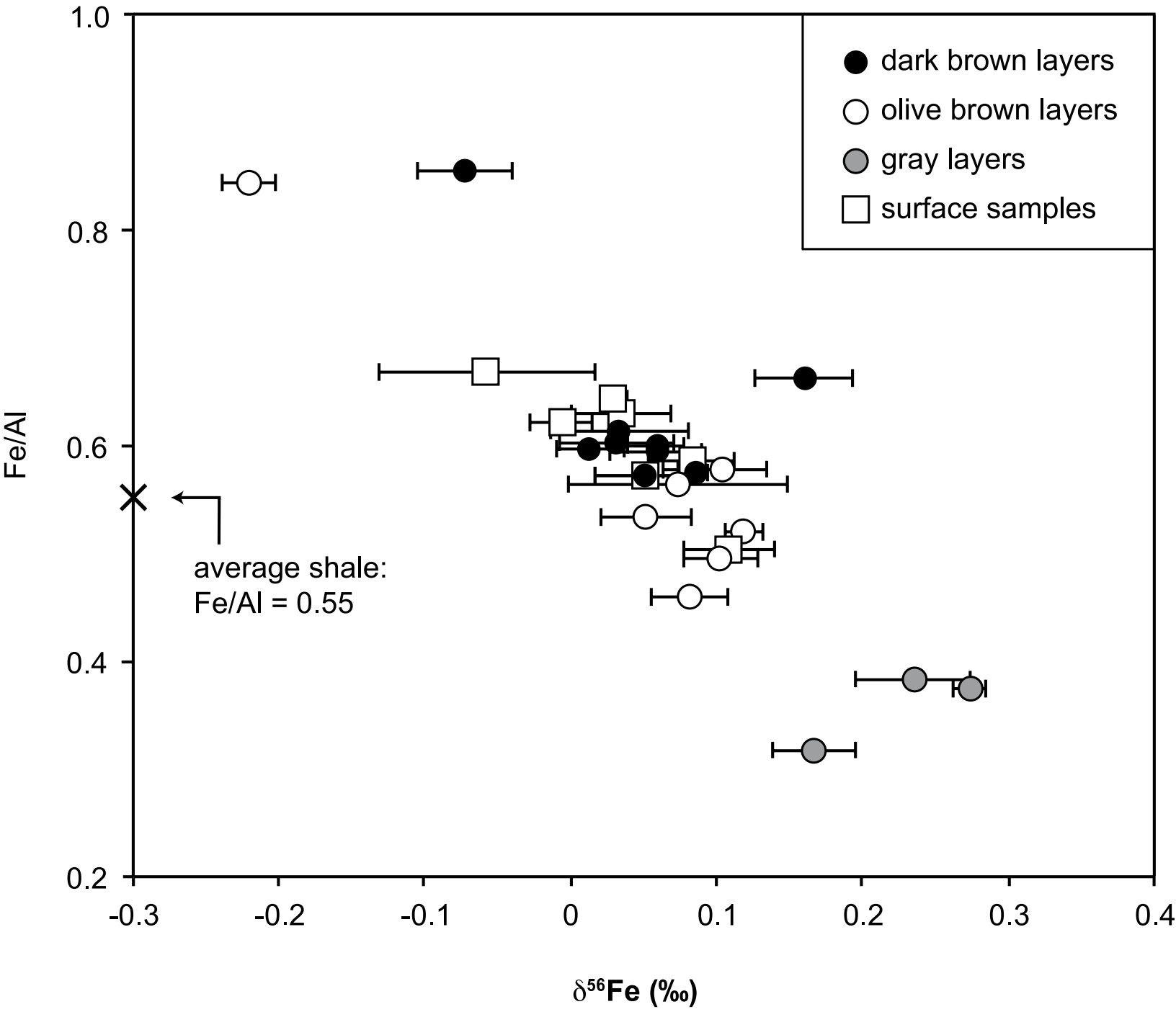
1.0
0.8
0.6
0.4
0.2
Fe/Al
-0.3
-0.2
-0.1
0
0.1
0.2
0.3
0.4
δ56Fe (‰)
dark brown layers
olive brown layers
gray layers
surface samples
average shale:
Fe/Al = 0.55

Figure10

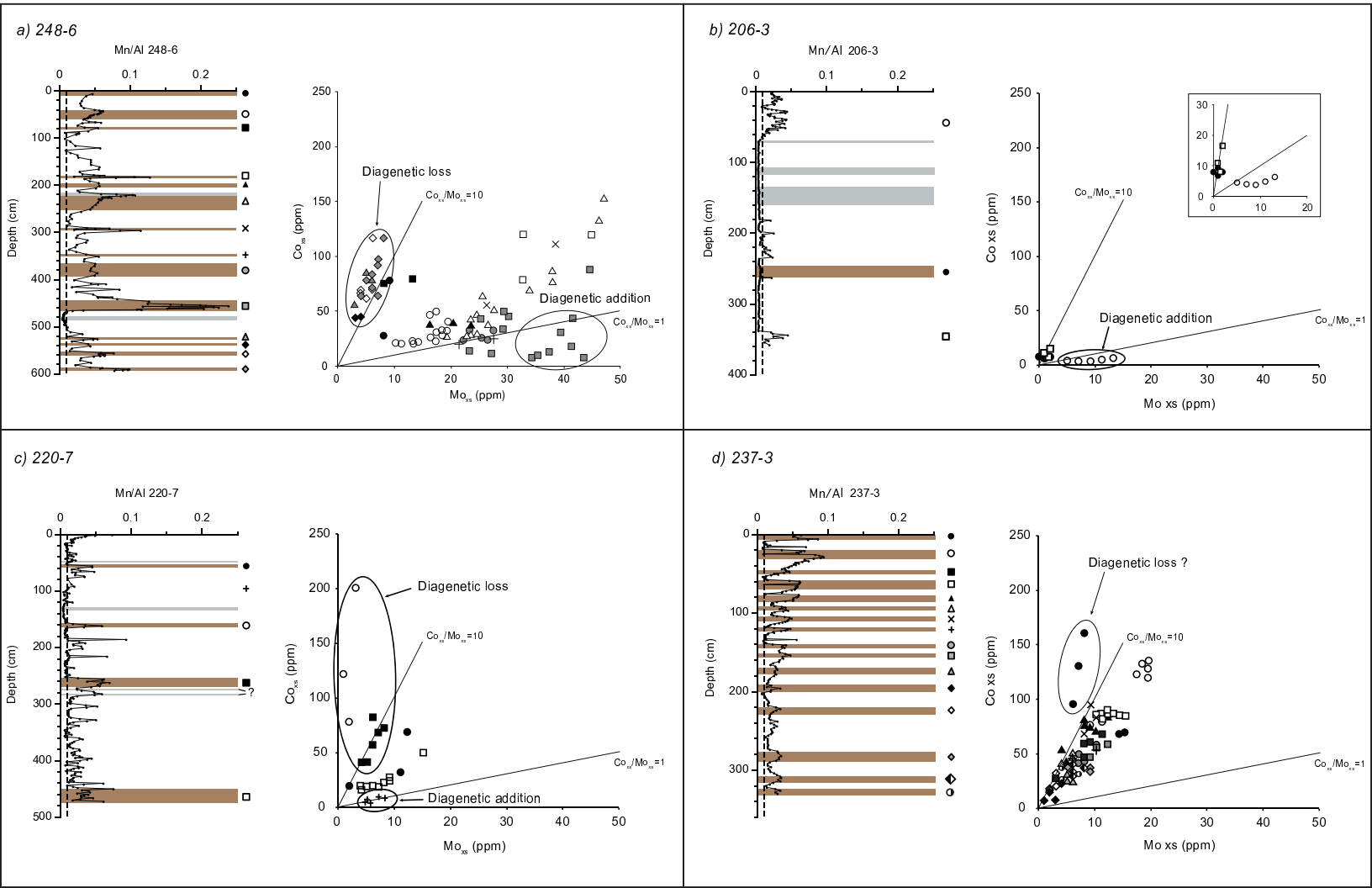
a) 248-6
Mn/Al 248-6
Depth (cm)
Diagenetic loss
Diagenetic addition
Mo_xs (ppm)
b) 206-3
Mn/Al 206-3
Co xs (ppm)
Mo xs (ppm)
c) 220-7
Mn/Al 220-7
d) 237-3
Mn/Al 237-3
Diagenetic loss ?

Figure11

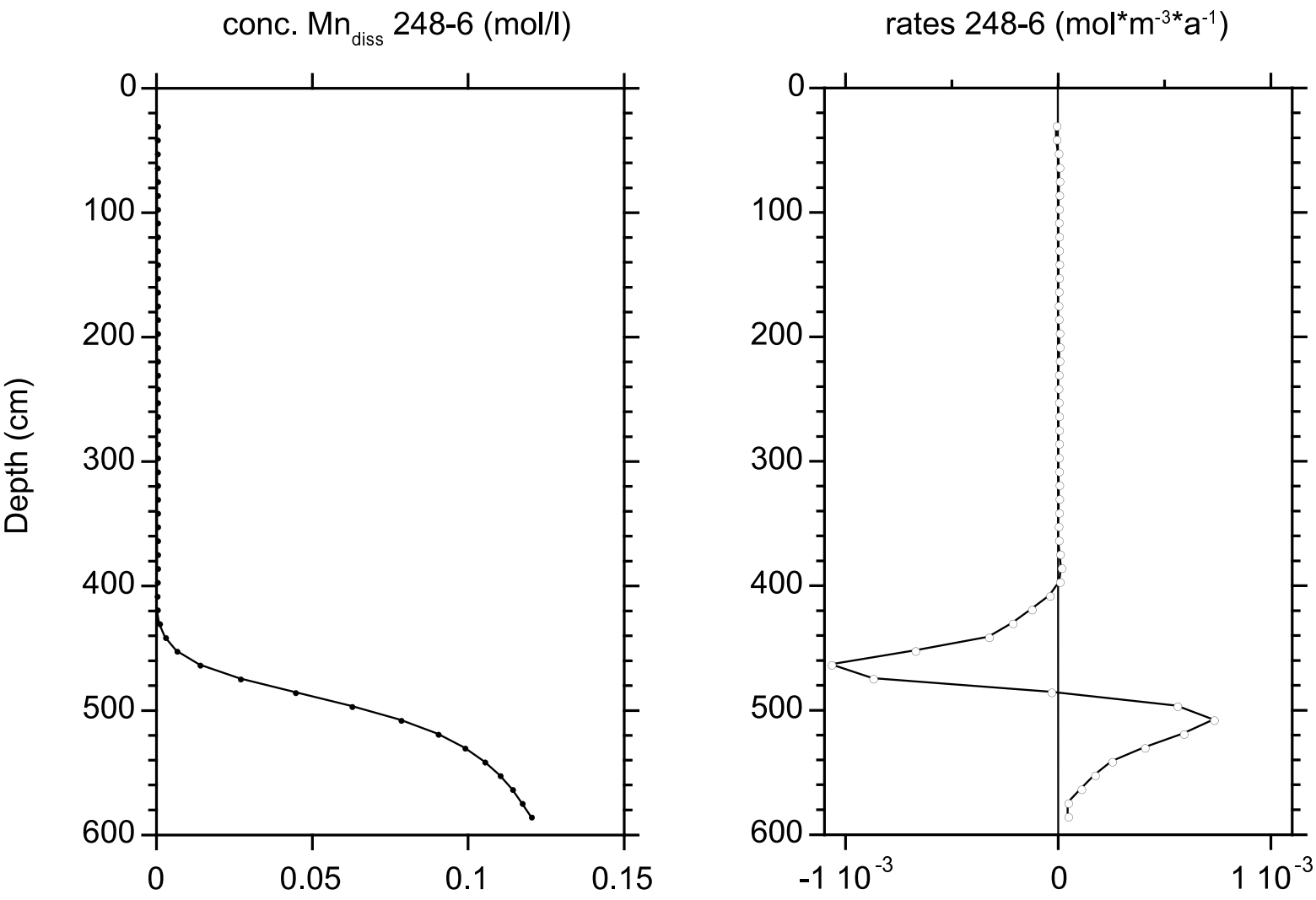
conc. Mn diss 248-6 (mol/l)
rates 248-6 (mol*m-3*a-1)
Depth (cm)
0
100
200
300
400
500
600
0
0.05
0.1
0.15
-1 10-3
0
1 10-3

Appendix

Click here to download Appendix: Appendix.docx